

AD-773 168

THE RELATIONSHIPS OF STRUCTURE TO  
PROPERTIES IN GRAPHITE FIBERS. PART II

Russell J. Diefendorf, et al

Rensselaer Polytechnic Institute

Prepared for:

Air Force Materials Laboratory

October 1973

DISTRIBUTED BY:

**NTIS**

National Technical Information Service  
U. S. DEPARTMENT OF COMMERCE  
5285 Port Royal Road, Springfield Va. 22151

DOCUMENT CONTROL DATA - R&D		
(Security classification of title, body of abstract and indexing annotation must be entered when the overall report is classified)		
1. ORIGINATING ACTIVITY (Corporate author)		2a. REPORT SECURITY CLASSIFICATION
Rensselaer Polytechnic Institute Materials Division, Troy, New York 12181		Unclassified
		2b. GROUP
3. REPORT TITLE		
THE RELATIONSHIPS OF STRUCTURE TO PROPERTIES IN GRAPHITE FIBERS		
4. DESCRIPTIVE NOTES (Type of report and inclusive dates)		
Final Report May 1971 to April 1972		
5. AUTHOR(S) (Last name, first name, initial)		
Diefendorf, Russell J. Tokarsky, Edward W.		
6. REPORT DATE	7a. TOTAL NO. OF PAGES	7b. NO. OF REFS
October 1973	67-70	6
8a. CONTRACT OR GRANT NO.	8a. ORIGINATOR'S REPORT NUMBER(S)	
F33615-70-C-1530		
b. PROJECT NO. 7342		
Task No. 734202		
c.	8b. OTHER REPORT NO(S) (Any other numbers that may be assigned this report)	
d.	AFML-TR-72-153, Part II	
10. AVAILABILITY/LIMITATION NOTICES		
Approved for public release; distribution unlimited.		
11. SUPPLEMENTARY NOTES		12. SPONSORING MILITARY ACTIVITY
		Air Force Materials Laboratory (MBC) Wright-Patterson AFB, Ohio
13. ABSTRACT		
<p>Three dimensional structural models of several different carbon fibers with different precursor bases and representing a wide modulus range have been developed. In addition, a larger variety of commercially available carbon fibers and the newer high performance organic fibers have been studied.</p> <p>Results from the individual characterizations indicate that increasing fiber modulus is accompanied by development of thicker, straighter, more crystalline, and better aligned ribbons of graphite. Quantitative optical measurements on fibers indicate a very steep modulus gradient is present in fibers from skin to core such that when fibers are loaded in tension, most of the load is born by the skin.</p> <p>General studies indicate PAN fibers experience an inflection in density in the 30-50 Msi range while the density of hot stretched fibers is uniformly proportional to modulus. Basal spacing and stack height fluctuate in the region of the density anomaly for the PAN fibers inferring a degree of structural disordering which may be related to the strength anomaly. In addition, the preferred orientation versus modulus relations for PAN and rayon base fibers is different implying constant strain conditions in PAN.</p> <p>Modulus is directly proportional to preferred orientation in organic fibers, and compressive failure is caused by buckling of polymer chains.</p>		

# Security Classification

14	KEY WORDS	LINK A		LINK B		LINK C	
		ROLE	WT	ROLE	WT	ROLE	WT
	Carbon and graphite fibers structur-property relations three-dimensional structural models x-ray and electron diffraction						

## INSTRUCTIONS

1. **ORIGINATING ACTIVITY:** Enter the name and address of the contractor, subcontractor, grantee, Department of Defense activity or other organization (*corporate author*) issuing the report.

2a. **REPORT SECURITY CLASSIFICATION:** Enter the overall security classification of the report. Indicate whether "Restricted Data" is included. Marking is to be in accordance with appropriate security regulations.

2b. **GROUP:** Automatic downgrading is specified in DoD Directive 5200.10 and Armed Forces Industrial Manual. Enter the group number. Also, when applicable, show that optional markings have been used for Group 3 and Group 4 as authorized.

3. **REPORT TITLE:** Enter the complete report title in all caps. Enter in all cases should be unclassified. If a restricted title cannot be selected without classification, show title classification in all capitals in parentheses immediately following the title.

4. **DESCRIPTIVE NOTES:** If appropriate, enter the type of report, e.g., interim, progress, summary, annual, or final. Give the inclusion dates when a specific reporting period is covered.

5. **AUTHOR(S):** Enter the name(s) of author(s) as shown on the report. Enter last name, first name, middle initial. If a title, show rank and branch of service. The name of the principal author is an absolute minimum requirement.

6. **REPORT DATE:** Enter the date of the report as day, month, year, or month, year. If more than one date appears on the report, use date of publication.

7a. **TOTAL NUMBER OF PAGES:** The total page count should follow normal pagination procedures, i.e., enter the number of pages containing information.

7b. **NUMBER OF REFERENCES:** Enter the total number of references cited in the report.

8a. **CONTRACT OR GRANT NUMBER:** If appropriate, enter the applicable number of the contract or grant under which the report was written.

8b, 8c, & 8d. **PROJECT NUMBER:** Enter the appropriate military department identification, such as project number, subproject number, system numbers, task number, etc.

9a. **ORIGINATOR'S REPORT NUMBER(S):** Enter the official report number by which the document will be identified and controlled by the originating activity. This number must be unique to this report.

9b. **OTHER REPORT NUMBER(S):** If the report has been assigned any other report numbers (either by the originator or by the sponsor), also enter this number(s).

10. **AVAILABILITY LIMITATION NOTICES:** Enter any limitations on further dissemination of the report, other than those

imposed by security classification, using standard statements such as:

- (1) "Qualified requesters may obtain copies of this report from DDC."
- (2) "Foreign announcement and dissemination of this report by DDC is not authorized."
- (3) "U. S. Government agencies may obtain copies of this report directly from DDC. Other qualified DDC users shall request through \_\_\_\_\_."
- (4) "U. S. military agencies may obtain copies of this report directly from DDC. Other qualified users shall request through \_\_\_\_\_."
- (5) "All distribution of this report is controlled. Qualified DDC users shall request through \_\_\_\_\_."

If the report has been furnished to the Office of Technical Services, Department of Commerce, for sale to the public, indicate this fact and enter the price, if known.

11. **SUPPLEMENTARY NOTES:** Use for additional explanatory notes.

12. **SPONSORING MILITARY ACTIVITY:** Enter the name of the departmental project office or laboratory sponsoring (paying for) the research and development. Include address.

13. **ABSTRACT:** Enter an abstract giving a brief and factual summary of the document indicative of the report, even though it may also appear elsewhere in the body of the technical report. If additional space is required, a continuation sheet shall be attached.

It is highly desirable that the abstract of classified reports be unclassified. Each paragraph of the abstract shall end with an indication of the military security classification of the information in the paragraph, represented as (TS), (S), (C), or (U).

There is no limitation on the length of the abstract. However, the suggested length is from 150 to 225 words.

14. **KEY WORDS:** Key words are technically meaningful terms or short phrases that characterize a report and may be used as index entries for cataloging the report. Key words must be selected so that no security classification is required. Identifiers, such as equipment model designation, trade name, military project code name, geographic location, may be used as key words but will be followed by an indication of technical context. The assignment of links, roles, and weights is optional.

AD773168

THE RELATIONSHIPS OF STRUCTURE TO PROPERTIES  
IN GRAPHITE FIBERS  
PART II

Russell J. Diefendorf  
Edward W. Tokarsky  
Rensselaer Polytechnic Institute

TECHNICAL REPORT AFML-TR-72-133, PART II

October 1973

Approved for public release; distribution unlimited.

1.c


## FOREWORD

This report was prepared by R. J. Diefendorf and E. W. Tokarsky, Materials Division, Rensselaer Polytechnic Institute; project 7342, "Fundamental Research on Macromolecular Materials and Lubrication Phenomena", Task 734202, "Studies on Structure-Property Relationships of Polymeric Materials" under contract AF33(615)-70-C-1530 entitled "The Relationship of Structure to Properties in Graphite Fibers". It was administered by the Air Force Materials Laboratory, Air Force Systems Command, Wright-Patterson Air Force Base, Herbert M. Ezekiel (AFML/MBC), project monitor.

Gratefully acknowledged is the scanning electron microscopy work of Mr. John Nelson, now of the Corning Glass Works. Special thanks is due Mr. W. Butler and Mr. W. Hunn of E. Leitz Inc. for kind permission to use a Leitz MPV System for special optical measurements. Samples of polyacetylene base fibers were supplied through Dr. D. G. Flom, General Electric Research and Development Center. Also, special thanks are due to Mr. J. Ray and H. Ezekiel of the Air Force, who supplied samples and data on high performance organic and experimental carbon fibers respectively.

This report covers research conducted during the period May 1971 to April 1972.

This report was submitted by the authors in July 1973. This technical report has been reviewed and is approved.

  
THEODORE J. REINHART, JR., CHIEF  
Composite & Fibrous Materials Branch  
Nonmetallic Materials Division

## TABLE OF CONTENTS

Section	Page
I INTRODUCTION	1
II EXPERIMENTAL TECHNIQUES	7
1. X-Ray Diffraction	8
2. Electron Diffraction	9
3. Electron Microscopy	9
4. Scanning Electron Microscopy	10
5. Polarized Light Analysis	10
6. Reverse Radio Frequency Sputtering	10
7. Bulk Densities of Fibers	10
8. Carbon Fibers	11
III RESULTS AND DISCUSSION	14
1. Individual Carbon Fibers	14
A. CS-5 Characterization	14
B. CS-7 Characterization	31
C. G.E. Monofilament Characterization	39
2. General Studies of Carbon Fibers	39
A. Density Results	39
3. Organic Fibers	50
REFERENCES	61

# LIST OF FIGURES

	Page
Fig. 1 Bright Field Fracture Profile, CS-5, $10\text{cm} = 3.0\mu$ .	15
Fig. 2 Electron Diffraction Pattern, CS-5	16
Fig. 3 (0002) Electron Dark Field of a CS-5 Fiber Exhibiting Modulation of $(10\bar{1}0)$ , $1\text{ cm} \approx 835\text{\AA}$	13
Fig. 4 (0002) Electron Dark Field of a CS-5 Fiber <u>not</u> Exhibiting Modulation of the $(10\bar{1}0)$ , $1\text{ cm} \approx 700\text{\AA}$	19
Fig. 5 Extraction Replica, CS-5, $1\text{ cm} \approx 0.15\mu$	21
Fig. 6 Longitudinal Sections, CS-5, Polarized Light, $1\text{ cm} \approx 2.2\mu$ .	22
Fig. 7 Extraction Replica, CS-5, Longitudinal Section after Reverse R-F Sputtering, $1\text{ cm} \approx 0.4\mu$	23
Fig. 8 Transverse Sections CS-5, Polarized Light, $1\text{ cm} \approx 4.5\mu$	24
Fig. 9 Schematic of Radial Distribution, CS-5	27
Fig. 10 Schematic of Radial Modulus Distributions, CS-5	28
Fig. 11 Three Dimensional Structural Model, CS-5	29
Fig. 12 (0002) Electron Dark Field, CS-7, $1\text{ cm} \approx 0.4\mu$	32
Fig. 13 Transverse Sections, CS-7 Polarized Light, $1\text{ cm} \approx 10\mu$	34
Fig. 14 Schematic Illustrations of the Two Types of Radial Preferred Orientations found in CS-7 Fibers	36
Fig. 15 Scanning Electron Micrograph, CS-7 Fibers R-F Sputter Etched in an Epoxy Matrix, $1\text{ cm} \approx 0.8\mu$	37
Fig. 16 Three Dimensional Structural Model, CS-7	38
Fig. 17 Three Dimensional Structural Model, G.E. Monofilament	40
Fig. 18 Modulus vs. Density of a Wide Range of Carbon Fiber	41

	Page
Fig. 19 Basal Spacing, $d_{0002}$ , vs. Modulus of Fibers	43
Fig. 20 Basal Stack Height, $l_c$ , vs. Fiber Modulus	45
Fig. 21 Basal Stack Height, $l_c$ , vs. Basal Spacing, $d_{0002}$	46
Fig. 22 Index of Preferred Orientation, $W_{1/2}$ vs. Fiber Modulus	48
Fig. 23 Optical Micrograph Failure Zone in Compression Tested PRD-49-I - Epoxy Composite, $1\text{ cm} \approx 100\mu$	52
Fig. 24 Higher Magnification of Sample in Fig. 23 in Polarized Light, $1\text{ cm} \approx 4.5\mu$	54
Fig. 25 Electron Bright Field, PRD-49-I Fracture Profile, $1\text{ cm} \approx 0.6\mu$	55
Fig. 26 X-Ray Pinhole Photograph of a Collimated Bundle of PRD-49-I Fibers	56
Fig. 27 X-Ray Pinhole Photograph of a Collimated Bundle of Fiber B Fibers	57
Fig. 28 Montage of Optical Micrographs of Polished Cross Sections of Organic Fibers in Reflected Polarized Light, $1\text{ cm} \approx 10\mu$	58

#### TABLES

Table I List of Fibers studied in the project	13
Table II Du Pont Aromatic Polyamid Yarn Properties	51



## SECTION I

### INTRODUCTION

The potential low cost of high performance carbon fibers has increased interest in filamentary reinforced composites for use in near term aerospace applications. While many suppliers are currently able to provide a wide variety of types of carbon fibers with a considerable range of mechanical properties, a number of technical problems remain. One of the most important is the lack of significant advances in increasing the strain to failure of the fibers, particularly for higher modulus fibers. Such a situation is partly responsible for the limited confidence placed in fabricated carbon composite members. A second major limitation has been the cost of carbon fibers, but processes producing cheaper fibers have also given poorer fiber properties. Little has been done to determine the causes of these poor properties. With few exceptions approaches to solutions have been mostly empirical. More rapid progress towards the solutions of these problems might be made by finding the pertinent structural features causing poor strength rather than through further trial and error development.

In Part I of this study, a limited number of carbon fibers prepared from several precursors and covering a wide range of elastic moduli were characterized in three-dimensions, and some consequences of these structures on the observed mechanical properties were developed.

It was concluded that carbon fibers consist of long undulating and twisting ribbons. For fibers with a modulus of 6 million psi., there is an almost random orientation of these ribbons with respect to the fiber axis. The thickness of these ribbons is approximately 5 to 6 turbostratic layer planes with a width of probably  $20\text{\AA}$ . The ribbons are highly undulated and twisted to give an inter-tangled mass. This provides a tight coupling between ribbons, and the fibers are observed to be surface flaw sensitive. Only a small portion of the surface appears to be covered with basal plane, and interfacial bonding to the matrix should be good. Flaw sensitivity should give a high gage length effect with tensile strength, with short gage lengths giving much higher strengths. Combined with good bonding, this should give a high "translation" of fiber strength (measured at 1 inch gage length) to the composite.

For fibers with a 40 million modulus, the ribbons are typically about 13 layer planes thick and  $40\text{\AA}$  wide. The amplitude of the undulation is greater than the wavelength, and about three-quarters of the basal planes are aligned within  $30^\circ$  of the fiber axis. Some variation in preferred orientation from the surface of the fiber to the center is observed, with the surface having a higher preferred orientation. There is also some radial preferred orientation with basal planes orienting parallel to the fiber surface. The radial preferred orientation in the center of the fiber depends on the processing, but is lower than the surface. The variation in axial

preferred orientation and the radial preferred orientation will give rise to residual stresses upon cool-down. These stresses are compressive axially and circumferentially at the surface, and tensile radially. The combination of radial residual stress with a lowered tangling of the ribbons gives poorer coupling between ribbons. Fractography also reveals rougher fracture surfaces. The lack of coupling of the ribbons and the compressive surface stresses also appear to make the fiber somewhat less flaw sensitive. However, tensile strength gage length effects are still relatively large. The fiber surface is starting to be covered with appreciable amounts of basal plane, but the resin bonding to the surface is still relatively high. The variation in axial preferred orientation will also cause the outside sheath of the fiber to carry more of the load. The interaction of this non-uniform loading with the residual stress has not been determined. The good bonding and high tensile strength at short gage lengths should give good "translation" of 1 inch gage length fiber strength to the composite.

For 50 million psi fiber, the ribbons remain turbostratic and increase to about 20 layers thick and  $70\text{\AA}$  wide. The undulation amplitude drops to less than the wavelength, and three quarters of basal planes are oriented within  $12^\circ$  of the fiber axis. Less tangling is observed between ribbons, and a high radial preferred orientation is observed with the basal planes parallel to the surface. The residual stress which develops from the radial

preferred orientation becomes high enough to cause internal fracture, which, with less tangling of the ribbons, gives poor coupling between ribbons. Fiber fracture surfaces become quite rough, and the tensile strength of the fiber often decreases. Flaw sensitivity and tensile strength gage length effects decrease. The surface of the fiber is predominantly a faulted basal plane, and interfacial bond strength, without etching, will be low. Translation of fiber tensile strength, for surface treated specimens, to composite properties will be reduced as the strength at short gage length does not increase as rapidly as for flaw sensitive fibers of lower modulus.

Finally, for fibers of 100 million modulus, the ribbons are about 30 layers thick and 90Å wide, but ribbon fusion is evident in some samples. For one PAN sample, three dimensional ordering was observed, together with a preferred orientation of a-axes. The orientation was that expected if the orientation of carbon backbone of the PAN polymer was retained throughout processing. The ribbons are observed to have almost zero amplitude and are essentially parallel to the fiber axis. Very little tangling is also observed. Strong radial preferred orientation occurs, and the resulting residual stresses must give very poor coupling between ribbons. Fracture surfaces are extremely jagged. The fiber surface consists of extremely smooth basal planes which would give poor bonding.

The strong similarities among carbon fibers of the same modulus,

but from different precursors, were more noteworthy than the differences. Axial structures appeared very similar with catalytically processed fibers having somewhat larger  $l_c$  values; differences were more apparent in radial structures. In general, however, higher radial preferred orientations were associated with higher axial preferred orientations. Samples which appear to be strain-annealed, i.e., fibers which have been strained at high temperatures by an applied stress, show a somewhat poorer development of radial structure as might be expected. In this case, the applied stress causes the basal planes to align parallel to the applied stress.

Finally, improved carbon fibers are conceivably possible if axial alignment of ribbons can be accomplished with a minimum of radial alignment. This would minimize decoupling of ribbons. In this second period, the relationship between structure and properties for a larger number of fibers, particularly commercially available carbon fibers, has been investigated. Also, this study has included more recently received samples of DuPont's wholly organic PRD-49 and Fiber B series.

Past work has shown that significant amounts of residual stress may be present in carbon fibers, and this will seriously affect flaw sensitivity. Secondly, the structural features responsible for residual stress make uniform loading of each fiber difficult, if not impossible. On a finer scale, little is known about the mechanisms of stress transfer among the rippled ribbon-shaped fibrils which compose all carbon fibers. In this regard, work done by Brydges et al <sup>1</sup> indicates that the elastic

moduli of carbon fibers lie between constant stress and strain models, while for practically all other types of carbon, the constant stress model appears to fit data well.

A different set of problems exists for the organic fibers. While uniaxial tensile properties are outstanding, compressive strength, composite interfacial shear strength, and machinability parallel to the fiber lay-up are serious deficiencies.

The purpose of this second part of the study has been: 1) to structurally characterize a wider range of carbon fibers while continuing further efforts to probe more deeply into the nature of carbon fiber structural features; 2) to structurally characterize the new organic fibers; and 3) to relate structure to properties in both cases.

To this end three carbon fiber samples were characterized in detail, three dimensional structural models developed, and consequences noted. Included in this part of this report are:

<u>Fiber</u>	<u>Modulus Msi</u>	<u>Precursor</u>
CS-5	116	Dralon T
CS-7	36.5	Courtelle
G.E. Monofilament	45	Polyacetylene

In the next part, results of more general studies on a wider range of carbon fibers are reported and analyzed. In the third part, the work on the organic fibers is given relating structure to properties.

## SECTION II

### EXPERIMENTAL TECHNIQUES

Structural features which have effects on the ultimate performance of carbon as well as organic fibers occur at various dimensional levels from the atomic or unit cell size to the level of the fiber diameter. Accordingly, the use of a number of experimental techniques is necessary to maximize resolution at each respective magnification

For both carbon and organic fibers, a principal emphasis is to describe preferred orientations of either the basal planes or aligned molecular chains, since the extent of such textures and their distributions have first order effects on fiber properties. Changes in these overall fiber microstructures are often associated with changes in the atomic level relations such as crystallite size and interlayer spacings. These atomic parameters are also required as they determine the elastic constants. For carbon, the shear compliance,  $S_{44}$ , varies with the interlayer spacing,  $d_{0002}$ , quite strongly, and the elastic properties parallel to the fiber axis will depend on the average values and distributions of  $S_{44}$ , the shear compliance as determined by  $d_{0002}$ . At the other extreme of magnification, e.g. the fiber diameter,

it is necessary to know the cross-sectional shape of the fiber, its overall size, pattern of radial preferred orientation development, and the distribution of axial preferred orientation.

Many of these important details can be resolved by the following techniques:

1. X-ray diffraction
2. Electron diffraction
3. Bright Field, Dark Field and Replication Electron Microscopy
4. Scanning Electron Microscopy (SEM)
5. Optical Polarized Light Microscopy
6. Reverse R.F. Sputtering of Fibers
7. Bulk Density Measurements.

#### 1. X-Ray Diffraction

For a fiber  $10\mu$  or less in diameter, the total volume of the fiber provides the x-ray diffraction information. Pinhole photographs of bundles of collimated fibers enabled qualitative assessments to be made of preferred orientation, crystallite size, three-dimension order, and small angle scattering. Quantitative measurements of atomic spacings, crystallite sizes, and preferred orientation were made using a Norelco diffractometer. Instrumental broadening of the diffractometer traces were determined for carbon fiber work by running a very well annealed sample ( $3600^{\circ}\text{C}$  for 16 hours) of pyrolytic graphite. In cases where small crystallite sizes were present, corrections to the raw data were made essentially following the procedure of Heckman<sup>2</sup>. A description of this correctional scheme was given in Appendix I



of Part I.

## 2. Electron Diffraction

Because the penetration of a 50 kV electron beam is only hundreds of angstroms in carbon, information obtained is heavily weighted toward surface features of the fibers. A Hitachi 50 kV Model HS-7 electron microscope was employed to obtain the electron diffraction patterns of carbon fibers which were then qualitatively assessed for comparison with x-ray data. Additionally, electron diffraction was utilized for local crystallographic reference in electron microscopy. Electron diffraction could not be obtained for the organic fibers since the focused electron beam degraded the fibers severely.

## 3. Electron Microscopy

Carbon extraction replicas of carbon fibers were prepared using chromium as shadowing material. Such replicas provide high resolution of surface texture, particularly along the fiber sides.

The bright field technique was used to study profiles of carbon and organic fibers, and also for some high magnification studies of sufficiently thin fiber regions. The dark field technique was also employed in the study of the carbon fibers, particularly the (0002) dark field, since it provides information about basal preferred orientation; in addition, crystallite sizes could be measured directly.

#### 4. Scanning Electron Microscopy (SEM)

SEM provides magnifications intermediate between optical and electron microscopy. Textures of sides and fractured ends of fibers could be observed as well as overall composite fracture characteristics.

#### 5. Polarized Light Analysis

The interaction of vertically incident plane polarized light with polished cross-sections of fibers may be used to determine radial distributions. Using the optical theory described previously,<sup>3</sup> it has been possible to quantitatively characterize several fibers used in this study. Although the optical interaction has not been as well characterized for the organic fibers, the same principles apply and have been used in a more qualitative fashion.

#### 6. Reverse Radio Frequency Sputtering

Reverse R.F. sputtering techniques make it possible to progressively and controllably etch away fiber surfaces without apparent damage. During this process, inert gas ions bombard a target material, in this case fibers mounted in an epoxy matrix, under the influence of a controlled power R.F. field.

#### 7. Bulk Densities of Fibers

The densities of these fibers were measured using a CCl<sub>4</sub>-CHBr<sub>3</sub> density gradient column. Density was measured approximately 24 hours after initial immersion.

## 8. Carbon Fibers

Listed in Table I are the carbon fibers studied to date along with the tensile modulus data furnished by the suppliers. The fibers are grouped by precursor (Fayon, Courtelle, Orlon, and miscellaneous), and arranged within each group in order of increasing tensile modulus. Also listed are the densities, which were measured at R.P.I., and moduli corrected for density i.e.,  $(2.26/\text{fiber density}) \times E$ . Such a correction permits a clearer comparison of fibers, but assumes that the porosity is parallel to the fiber axis; in view of previous small angle scattering work done here as reported in Part I, this is not an unreasonable limiting assumption. Also included are the x-ray determined crystallographic parameters:

1. basal spacing,  $d_{0002}$
2. stack height  $l_c$
3. index of preferred orientation,  $W_{1/2}$

Information on the preparation procedures used for the commercial samples is proprietary for the most part. Fibers with the CS code designation were special experimental samples provided by Mr. H. M. Ezekiel.

### CS-1

CS-1 was prepared from an experimental PAN homopolymer, high tenacity, dry spun yarn. It was made by a direct graphitization technique (i.e. no carbonization step) and was not surface treated.

### CS-2

CS-2 was prepared from a wet spun experimental homopolymer in

the usual manner (i.e. full stabilization, carbonization, graphitization) and was surface treated.

#### CS-3

CS-3 was made from Villwyte rayon and was not surface treated.

#### CS-4

CS-4 was prepared from a commercial carbon yarn VYB 70- $\frac{1}{2}$  by a catalytic graphitization process (British provisional specification, 1,295,289) and was not surface treated.

#### CS-5

CS-5 was also prepared according to the same catalytic graphitization process as CS-4, but was made from a commercial PAN yarn, Dralon T, and was not surface treated.

#### CS-7

CS-7 was commercial HTS type carbon yarn.

#### General Electric Monofilament

The monofilament is an experimental fiber made from a polyacetylene precursor, and was developed at the General Electric Research and Development Center ; samples were provided through the courtesy of D. G. Flom.

TABLE I

RAYON BASE FIBERS

<u>Fiber</u>	<u>E, X 10<sup>6</sup>psi.</u>	<u>E<sub>corr.</sub></u>	<u><math>\rho</math></u>	<u>d<sub>0002</sub>, Å</u>	<u>l<sub>c</sub>, Å</u>	<u>W<sub>1/2</sub>, °</u>
WYB	6	10	1.40	3.416	19.6	61.0
Thornel 25	23	35	1.47	3.405	37.9	12.1
Thornel 50	46	63	1.63	3.401	47.0	8.1
Thornel 75	76	94	1.82	-	-	-
CS-4	88	107	1.86	3.37	155	7.5
CS-3	103	135	1.73	3.396	69.7	2.6

COURTELLE PAN BASE FIBERS

AS	31	39	1.80	3.410	13.8	29.5
Morganite II	34	43	1.79	3.413	18.1	23.5
CS-7	37	47	1.77	3.390	24.1	25.1
HTS	39	51	1.73	3.439	22.2	22.7
Fortafil 5-Y	55	65	1.91	3.390	61.1	16.3
HMS	56	67	1.88	3.390	55.4	13.8
Morganite I	65	76	1.94	3.388	93.4	7.8

ORLON PAN BASE FIBERS

Great Lakes 3T	30	38	1.80	3.414	12.7	29.7
Great Lakes 4T	38	48	1.80	3.400	21.4	25.8
Great Lakes 5T	48	59	1.85	3.384	33.5	19.6
Great Lakes 6T	58	69	1.90	3.354	57.5	11.2

ROUND PAN BASE FIBER

CS-2	41	55	1.69	3.433	16.8	28.3
------	----	----	------	-------	------	------

DOGBONE PAN BASE FIBERS

CS-1	100	106	1.95	3.357	115	5.9
CS-5	116	124	2.12	3.36	203	2.3

OTHER

G.E. Monofilament Polyacetylene	45	63	1.62	3.406	55.4	9.9
------------------------------------	----	----	------	-------	------	-----

### SECTION III

#### RESULTS AND DISCUSSION

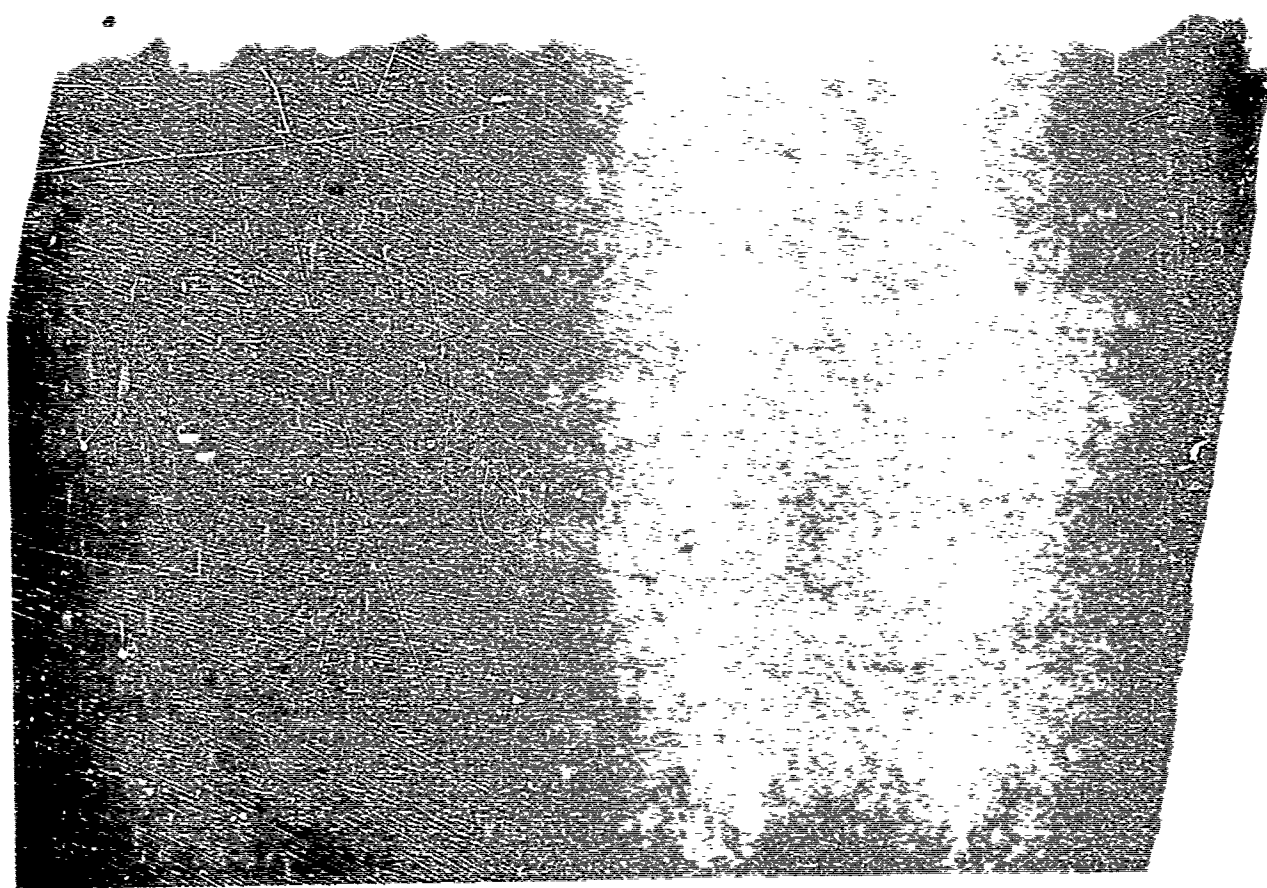
##### Part 1. Individual Carbon Fibers

##### A. CS-5 Characterization

CS-5 is a dogbone shaped carbon fiber having an axial tensile modulus of 116 Msi and was produced via the catalytic graphitization process from Dralon T precursor.

Shown in Fig. 1 is an electron bright field photograph of a CS-5 fiber fractured in bending. The very jagged fracture profile is indicative of a very high axial preferred orientation. This is in agreement with the previous hypothesis which suggested that as the microfibrils become better aligned, the shear coupling between them is reduced; and as a consequence, when the fiber is fractured cracks will be deflected for long distances between the ribbons since this is the path of least resistance.

Electron diffraction patterns of CS-5 fall into two categories depending on whether the  $(10\bar{1}0)$  is modulated. Shown in Fig. 2 is a pattern of the first type. The six spots indicate three dimensional ordering of part of the fiber from which the diffraction originated. It is significant that the six spot pattern is not symmetrically displaced with respect to the  $(0002)$  intensity maxima. The positions of these spots show that one of the "a" directions in the contributing microfibrils is displaced about  $15^\circ$  away from the  $(0002)$  axis of the ribbon as shown following:



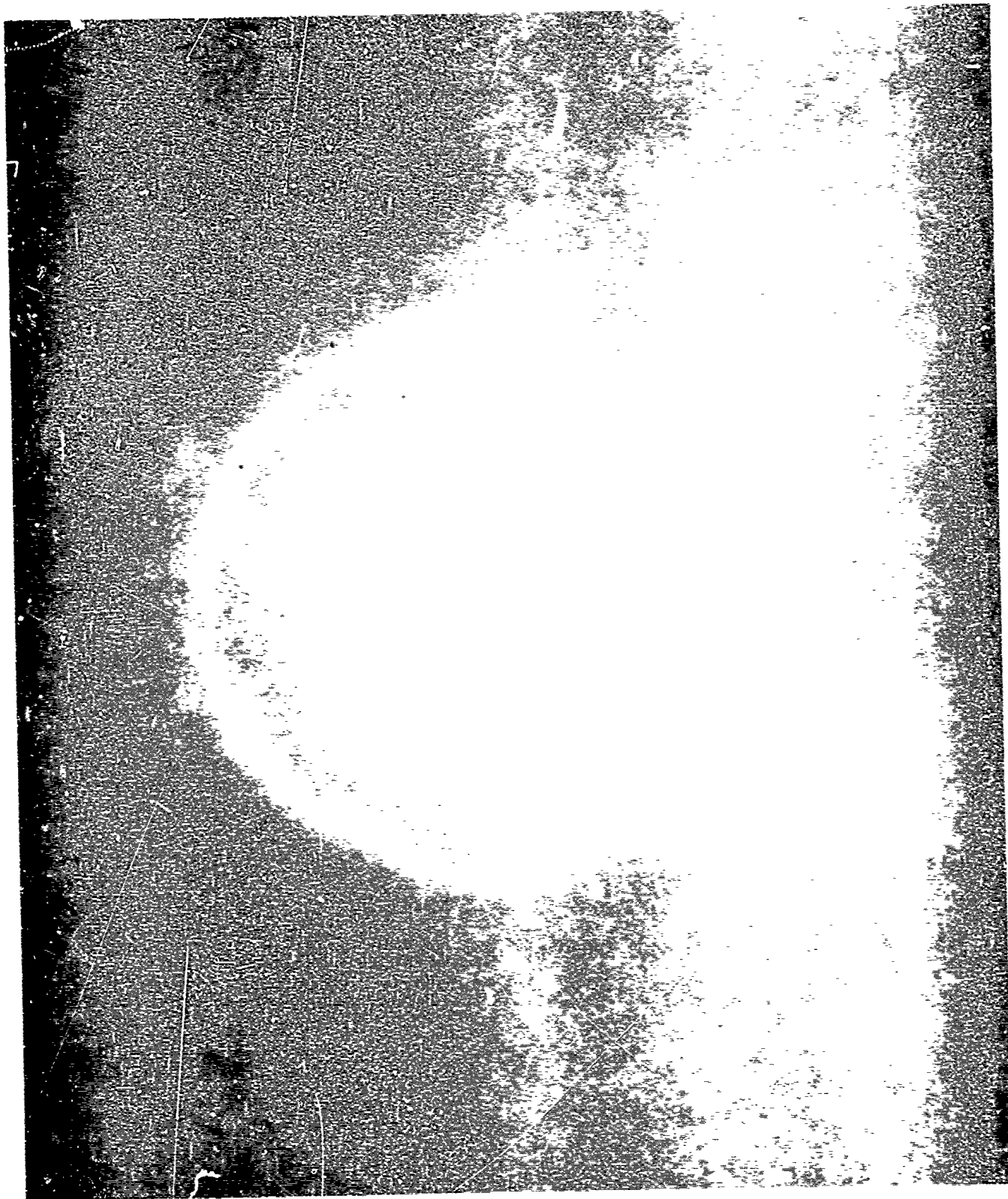
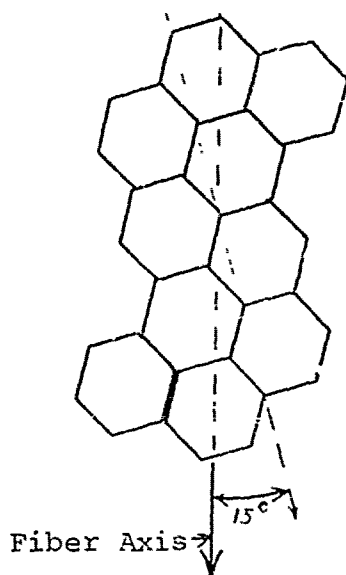


Fig. 2. Flo. 10.

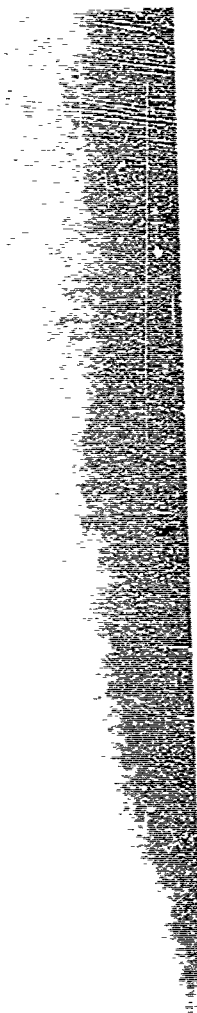
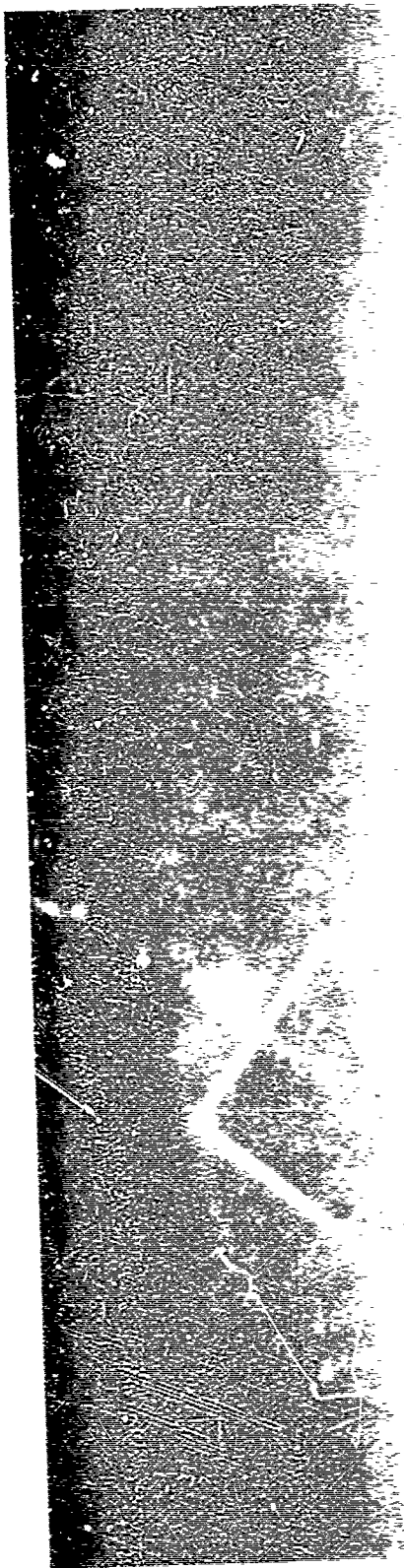




Because only a part of the  $(10\bar{1}0)$  intensity is concentrated in these six spots, it must be realized that the usual situation is that either no "a" axis preferred orientation exists or more probably, that the "a" axis cannot be determined because of the lack of three dimensional ordering.

The  $(0002)$  dark field of a section of a CS-5 fiber exhibiting modulation of the  $(10\bar{1}0)$  is shown in Fig. 3.  $L_c$  crystallite sizes ranging from about  $80\text{\AA}$  to over  $500\text{\AA}$  are present as well as axial  $l_a$  values in the micron range. The amplitude of the microfibril ripple, especially when compared to lower modulus fibers, is expected to be very small for such a high modulus fiber. Other areas of CS-5 which exhibited diffraction patterns of the second type gave rise to  $(0002)$  dark fields as exemplified in Fig. 4. In this case  $l_c$  is around  $150\text{\AA}$  while  $l_a$ , axially, again extends into the micron range. On the side of the fiber, some evidence exists for cross correlation of microfibril ripple, as indicated in the blocked area. This may illustrate the first stage of





adjacent ribbon fusion, and would be expected to begin at the fiber surface. That the surface itself is at least locally well developed is supported in Fig. 5, an extraction replica of the longitudinal surface of a single CS-5 fiber. The apparent smoothness accompanied by a striated texture is suggestive of high basal character.

To help clarify the possibility of a duplex microstructure, a bundle of CS-5 fibers was mounted in an epoxy matrix such that the fiber axes were approximately parallel to the specimen mounting surface; subsequent grinding and polishing produced longitudinal sections suitable for metallographic examination. Shown in Fig. 6 are such longitudinal sections of several fibers in reflected polarized light. The longitudinal surfaces of these fibers appear to be covered by a layer which behaves optically like a series of pyrolytic growth cones. Furthermore, the section of the layer in the blocked area appears to be either extraordinarily thick, or to have broken away implying that the bonding between the outer layer and fiber interior is not great. This separation may have occurred when the fiber bundle was broken in bending before mounting. Subsequently the sample was reverse RF sputtered and replicas of the surface were prepared. Fig. 7 is an extraction replica of such an etched longitudinal surface. Though a bit out of focus, the surface layer is similar to the pyrolytic-like morphology in the optical photomicrograph.



Fig. 5 Extraction Replica, CS-5, 1 cm  $\approx$  0.15 $\mu$



Fig. 1. Longitudinal sections, 10-15  
Polarized light, 100x magnification.



Fig. 7 Extraction Replica, CS-5, Longitudinal Section  
After Reverse R-F Sputtering, 1 cm  $\approx$  0.4 $\mu$

The extent to which this layer exists was revealed by polarized light microscopy of the cross section of a bundle of CS-5 fibers as shown in Fig. 8. Close inspection reveals that the characteristic optical activity pattern occurs only on fibers comprising the perimeter of the bundle. Further observations in the optical microscope suggest that the pyrolytic-like layer may in fact bridge some of the perimeter fibers, suggesting a redeposition origin. Another possibility which may explain the surface layer is that the catalytic graphitization procedure may not have been uniform, only affecting the outermost fibers of the bundle.

Further use of the reflected polarized light interaction enabled quantitative determinations of typical radial distributions in CS-5 fibers not possessing the surface layer. Quantitative measurements of rotation angles were made using the Leitz MPV microscope-photometer with a variable slit measuring diaphragm. This system enables the elliptical character of light reflected from areas as small as  $\frac{1}{2}$  micron on a side to be quantitatively determined. The combination of this information with careful evaluation of photographic data has led to the proposed radial distribution shown in Fig. 9a. It is clear that the overall symmetry is a significant departure from the largely onion skin textures seen previously<sup>3</sup>. It must be emphasized that radial distributions within the bundle studied varied; onion skin distributions were found, but were certainly not as dominant as has been



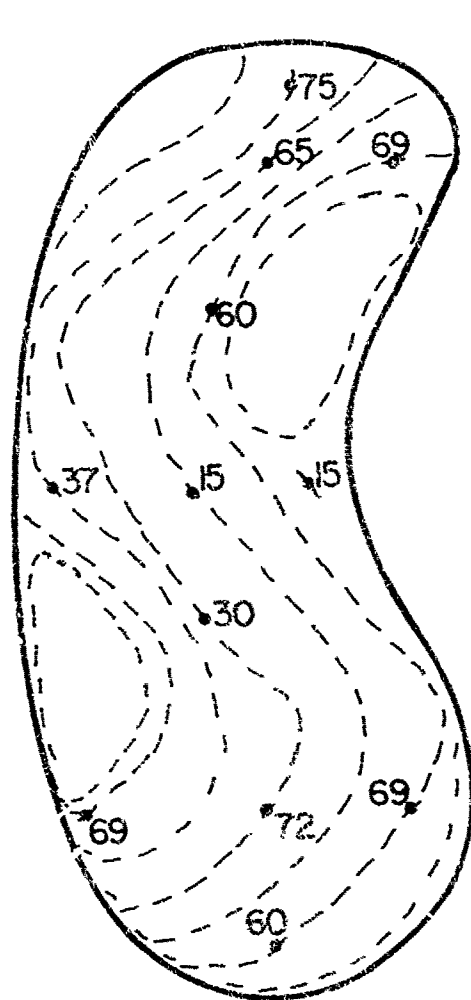


the case for lower modulus fibers studied. In particular, the central area between the lobes is oriented about 40-50° away from that expected of an onion skin type morphology. This microstructure is similar to an understabilized Courttelle PAN base carbon fiber where the outer stabilized surface region is onion-skin and the inner understabilized structure is radial. However, the authors do not know if the diffusion limited stabilization which apparently gives the duplex microstructure of Courttelle base fibers also holds for this Dralon T sample.

Given in Fig. 9b, also from optical measurements, are the contour lines representing zones of approximately constant axial tilt of the basal plane away from the fiber axis. The contour lines are drawn for 10° increments. It is apparent that the axial preferred orientation is very far from uniform; the highest axial orientation is found in the area between the lobes and decreases rapidly in the direction of the lobes. Each lobe appears to have developed its own concentric axial preferred gradient. Over much of the convex surface of the fiber is a very thin but highly aligned skin.

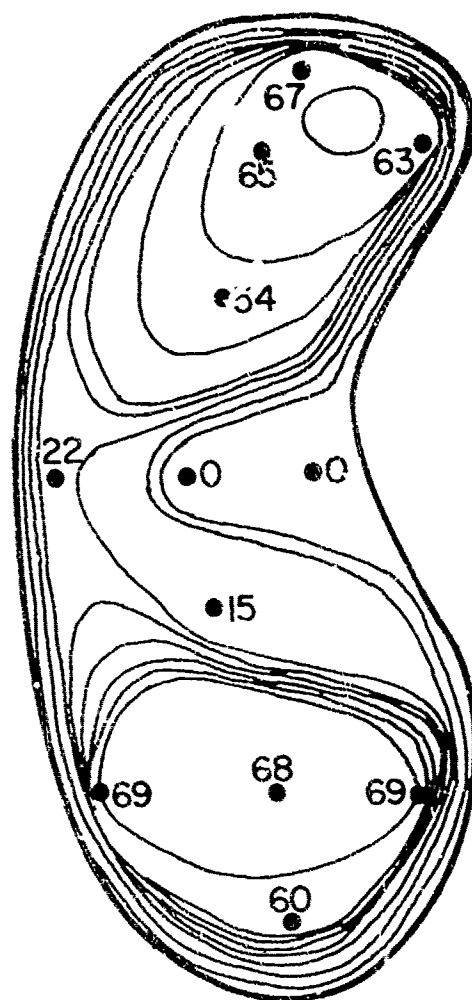
If a constant stress model is assumed for this fiber, and it is further assumed that the moduli within each region parallel to the fiber axis are functions only of the tilt of the basal plane, then the moduli may be calculated from the compliance transform:

$$S'_{11} = s_{11} \cos^4\phi + s_{33} \sin^4\phi + (s_{44} + 2s_{13}) \cos^2\phi \sin^2\phi$$



(a)

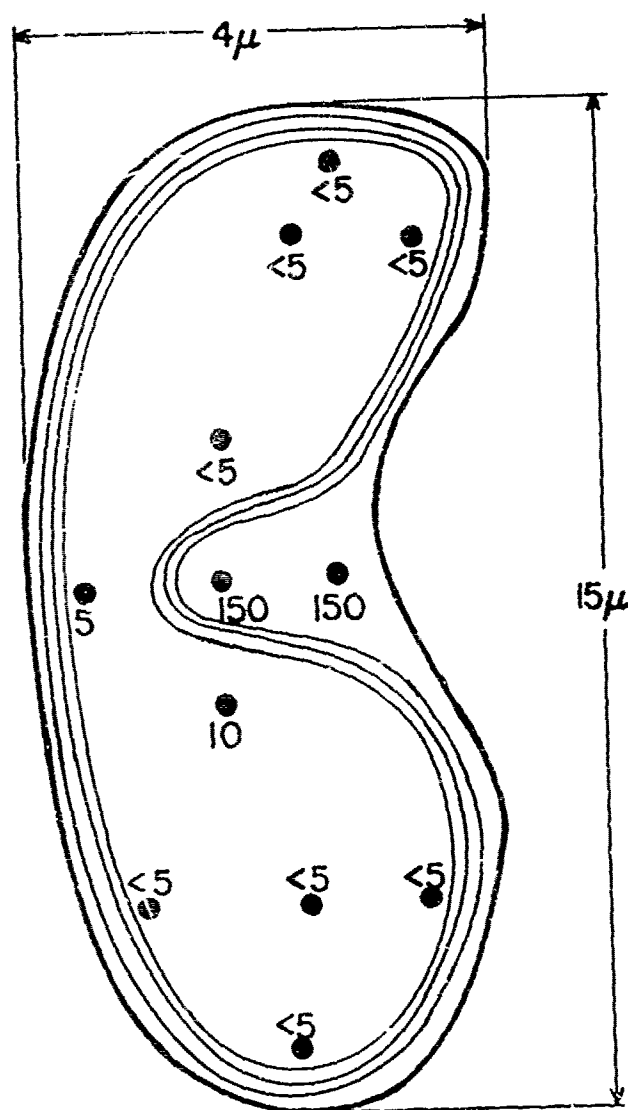
$\phi'$ s from experimental curve



(b)

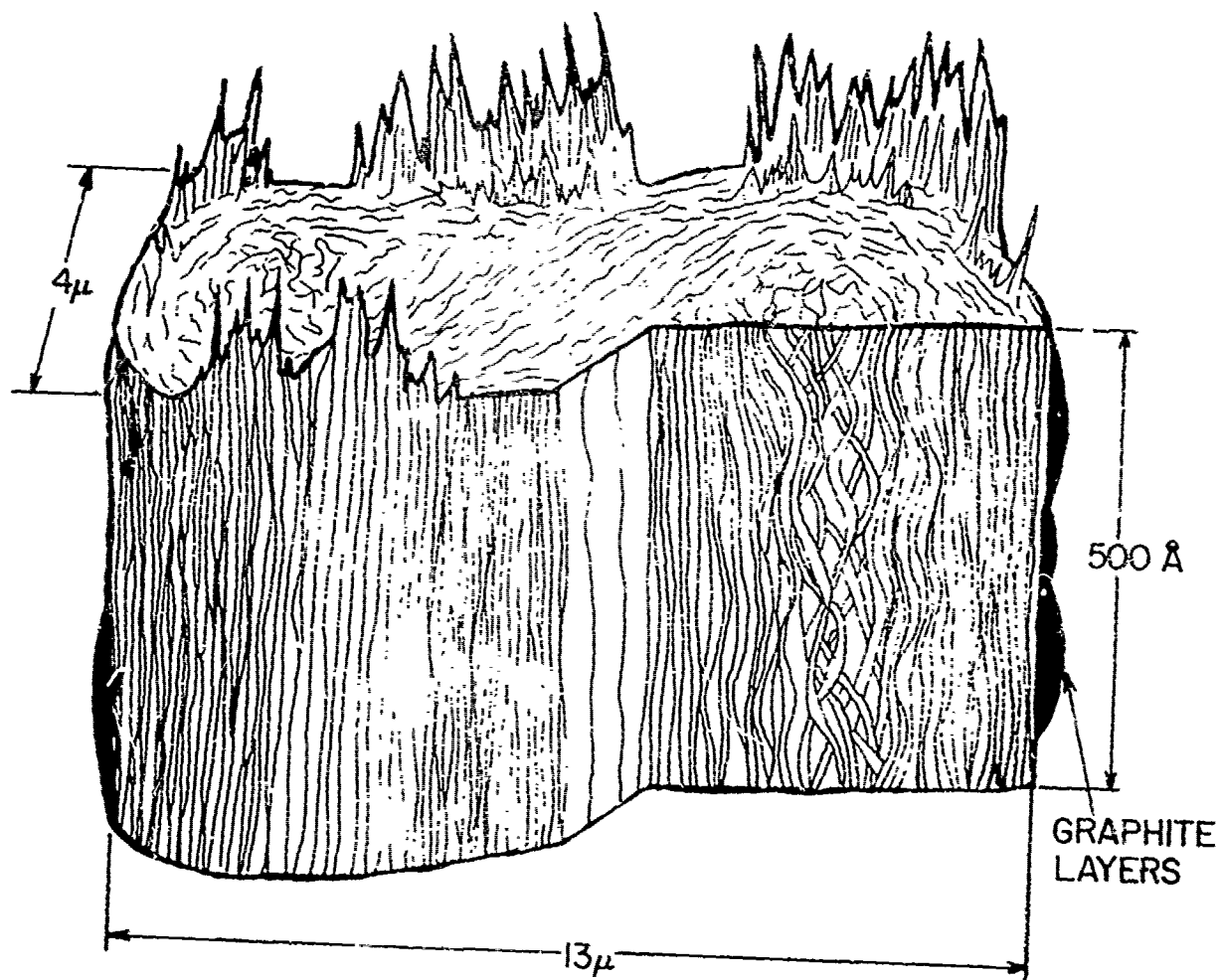
$\phi'$ s after correction for fiber tilt

Fig. 9 Schematic of Radial Distribution, CS-5



Numbers represent axial moduli values (in Msi) over the cross section of the fiber.

Fig. 10 Schematic of Radial Modulus Distributions, CS-5



CS-5

Fig. 11 Three Dimensional Structural Model, CS-5

where  $E = 1/s'_{11}$

For these calculations, the following elastic constants were used .

$$s_{11} = 9.85 \times 10^{-14} \text{ cm}^2/\text{dyne}$$

$$s_{33} = 275 \quad " \quad " \quad "$$

$$s_{44} = 2500 \quad " \quad " \quad "$$

$$s_{13} = -3.3 \quad " \quad " \quad "$$

Such calculations lead to the modulus contour configuration given in Fig. 10; the contours are drawn for each increment of 50 Msi. It was stated earlier that the overall radial structure of CS-5 was not onion skin; however, while the orientation of the basal planes is a radical departure from fibers previously reported, a more or less concentric axial preferred gradient still exists. Furthermore, it is apparent that a very sharp modulus gradient results from such a distribution of  $\phi$ 's, and will be a source of residual stress on cool-down. Additionally, the high modulus of the skin and central area of the fibers will make uniform loading difficult.

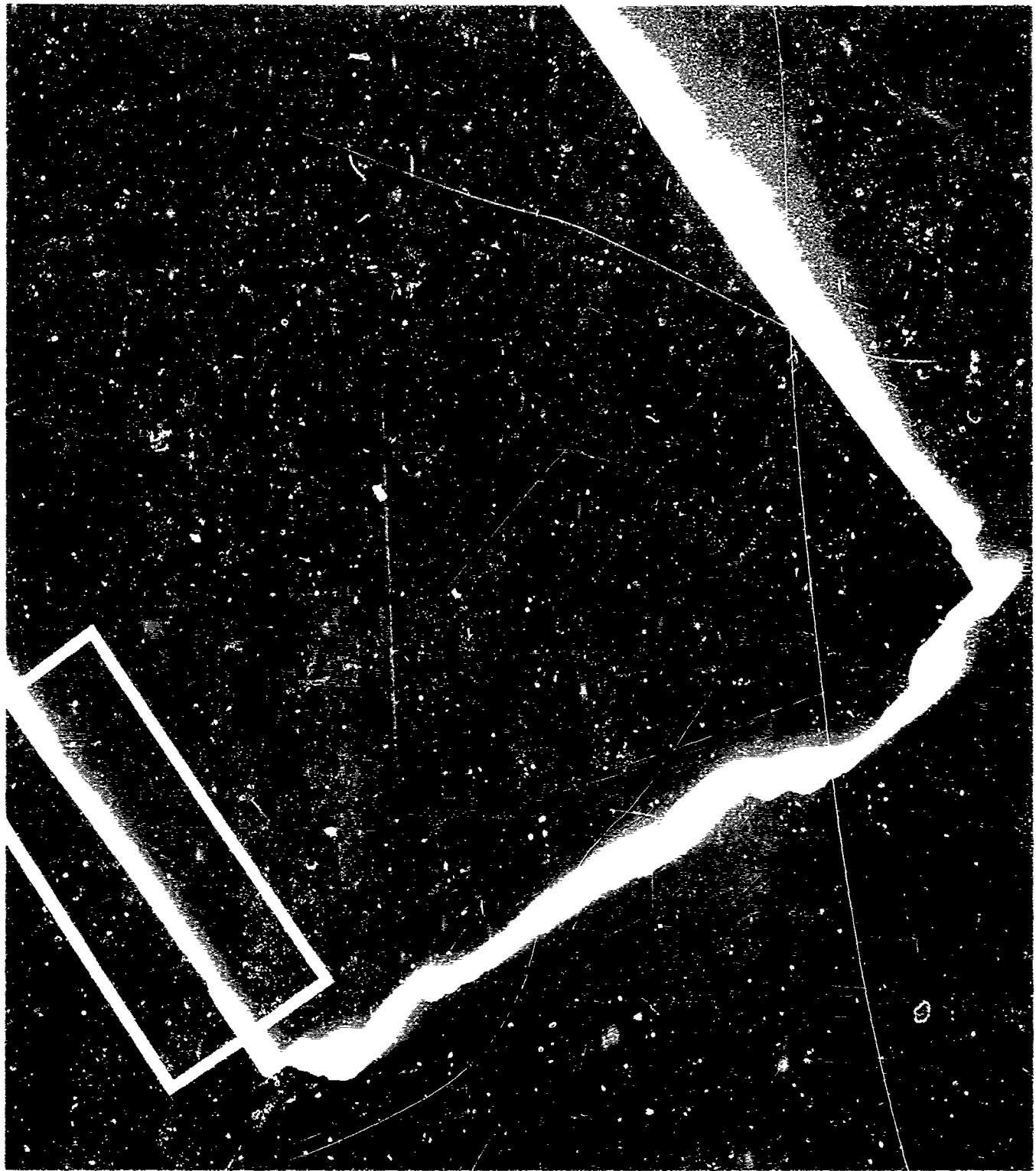
#### Summary of CS-5 Fiber

CS-5, a catalytically graphitized PAN based fiber, has a corrected modulus of 124 Msi; a three dimensional schematic model is shown in Fig. 11. X-ray preferred orientation measurements of aligned bundles of fibers indicate that about 2/3 of the basal planes are within  $2.3^\circ$  of the fiber axis. Electron diffraction measurements indicate that three dimensional order exists over

limited regions of the fiber, particularly the surface. The surface texture itself is relatively smooth, characteristic of a highly basal nature. (0002) dark field work indicates that a distribution in axial preferred orientation exists over the length of the fiber. Quantitative optical measurements confirm this, and also indicate that steep modulus gradients exist over the cross-section of the fiber. The overall radial symmetry is a radical departure from other fibers observed, although a very thin ( $< 0.5\mu$ ) onion skin is present. The poorest preferred orientation is found in the core of each lobe. The fibers at the perimeter of the bundle appear to be coated with a pyrolytic like layer which may explain the apparent poor preferred orientation appearance of the Debye Scherrer photographs.

#### B. CS-7 Characterization

Debye Scherrer photographs of CS-7 (early (HTS)) show that the fiber has relatively poor average axial preferred orientation relative to CS-5. Corrected quantitative measurements using a Norelco diffractometer indicate that the average basal spacing,  $d_{0002}$ , is  $340\text{\AA}$  while the stack height,  $l_c$ , as determined from the (0002) peak half width is about 12 basal layers. It can be inferred from electron diffraction patterns that while surface preferred axial orientation is present and better than the fiber volume average, it is not great. Furthermore, no evidence for three dimensional ordering exists. Shown in Fig. 12 is an (0002)





dark field photograph of a CS-7 fiber fractured in bending. No modulation of the light intensity is observed at the end; the bluntness of the end is an indication of overall poorer preferred orientation. The area in the block along the fiber side is evidence for relatively poor longitudinal structural development since the intensity is lower in this local region. In addition, the other longitudinal surface does show some small scale intensity variations, but these are not marked. This lack of higher structural development may be related to the fact that CS-7 has been surface treated.

Further information necessary for the development of radial distributions is found from optical polarized light microscopy. Shown in Fig. 13 are transverse sections of CS-7 fibers as seen when the nicols are at 90°. The cross sections of CS-7 fibers are approximately circular, and the diameter is approximately 10 $\mu$ , but fiber diameters as high as 15 $\mu$  are also observed. At least one extinction cross, which is due to form birefractance, is present in each fiber. The positions of the crosses remain relatively fixed with respect to the polarizer and analyzer when the microscope stage is rotated. This indicates primarily onion skin and/or spoke-like radial structure having the fiber axis as symmetry center. It is also apparent that the largest fibers possess a cross within a cross; close inspection reveals that the magnitude of this effect is proportional to the diameter of the fiber.

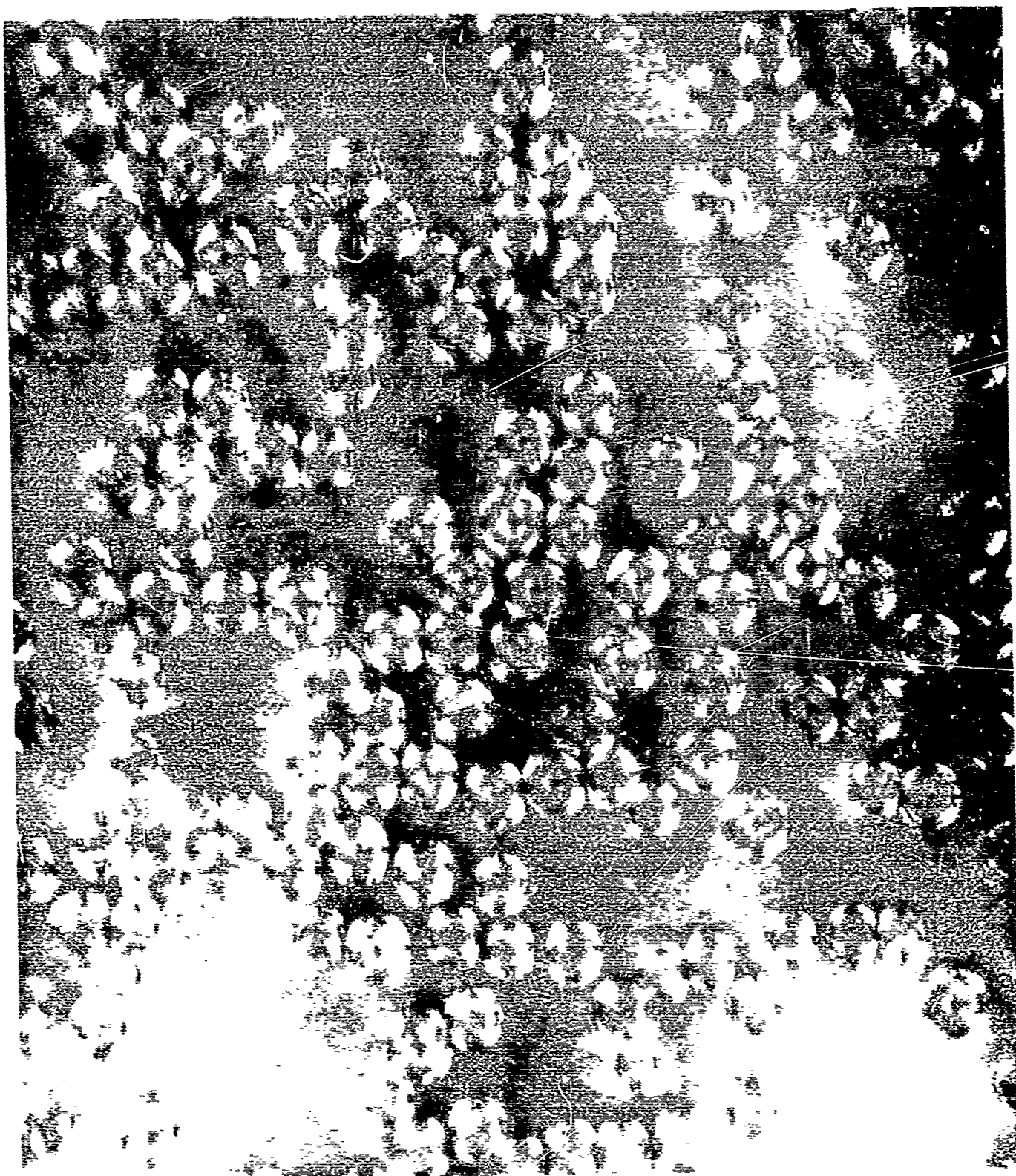


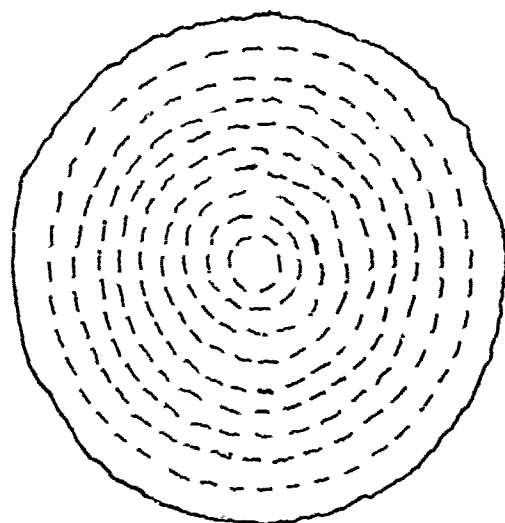
Fig. 13 Transverse sections, W-6  
Polarized light, 100x

Using techniques described in Part I of this report, it was determined that the overall radial structure of CS-7 is onion skin with a progressively better developed spoke configuration in the core for the larger diameter fibers. These models are illustrated in Fig. 14. The axial preferred orientation is better at the outside of the fiber since the form birefractance cross is more intense. The apparent rotation angle at the  $45^\circ$  position was about  $7^\circ$ , thus indicating that the average angle that the carbon micro-fibrils make with the fiber axis is approximately  $20^\circ$  near the surface.

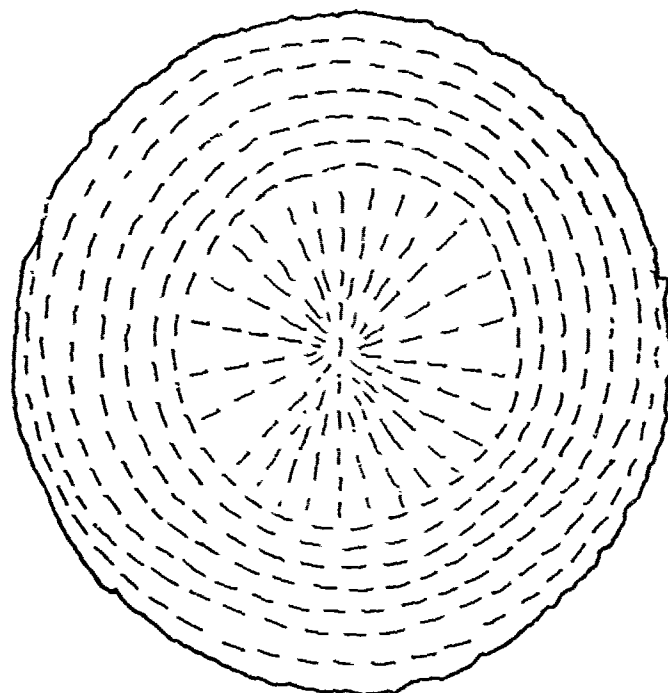
A scanning electron photomicrograph of a reverse R-F sputtered sample is shown in Fig. 15. The outside surfaces of the fibers have etched in a markedly different way, and delineated a highly preferred surface structure. Furthermore, the cores are dimpled, and this is probably related to either a different axial or radial preferred orientation, or both.

#### Summary of CS-7 Fiber

CS-7 is a circular cross section fiber which is actually an earlier produced sample of HTS; its three dimensional structural model is shown in Fig. 16. The basal spacings  $3.40\text{\AA}$  and the stack thickness is about 12 basal layers. CS-7 shows evidence of incomplete stabilization in contrast to HTS, and this may explain the difference in average basal spacing; overall however, the radial preferred orientation of CS-7 is onion skin with the basal planes making an angle of about  $20^\circ$  with respect to the fiber axis



ONION SKIN TEXTURE

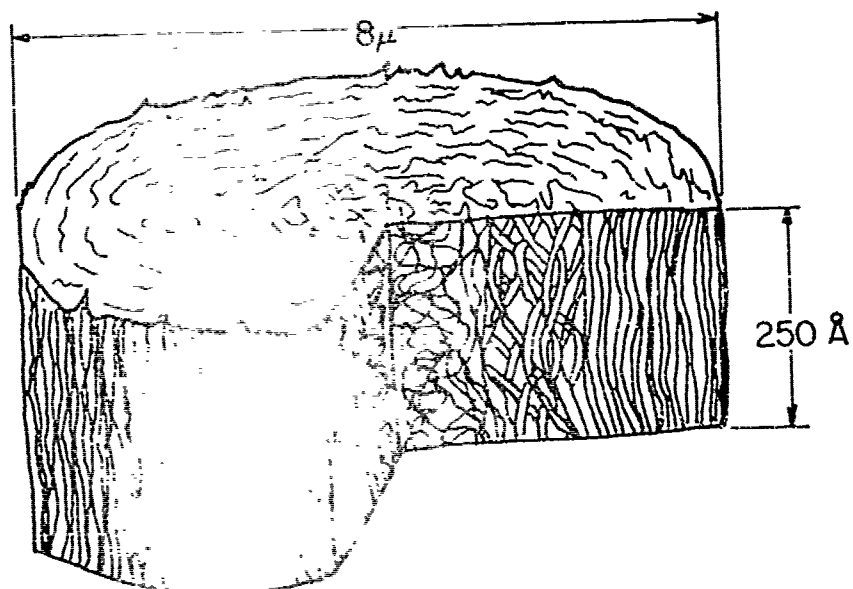


ONION SKIN WITH SPOKE CORE

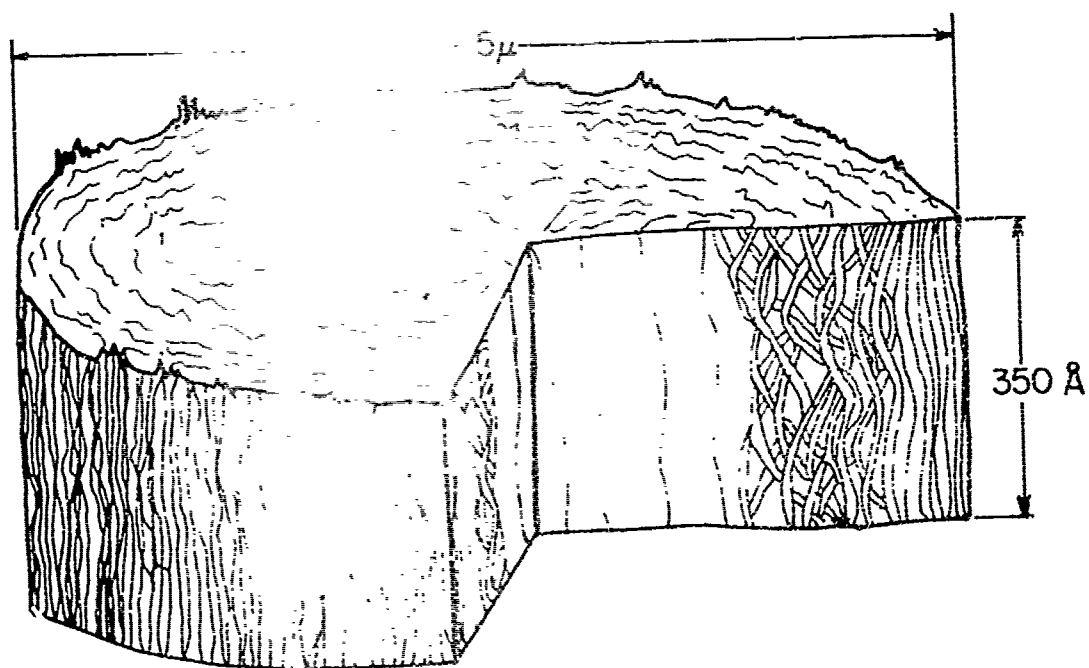
Fig. 14 Schematic Illustrations of the Two Types of Radial Preferred Orientations found in CS-7 Fibers



Fig. 15 Scanning Electron Micrograph, CS-7 Fibers  
R-F Sputter Etched in an Epoxy Matrix,  
1 cm  $\approx$  0.8 $\mu$



STABILIZED CS-7



IMPROPERLY STABILIZED CS-7

Fig. 16 The Structural Model, CS-7

at the fiber surface. These results are supported by differential etching rates of CS-7 in an RF plasma.

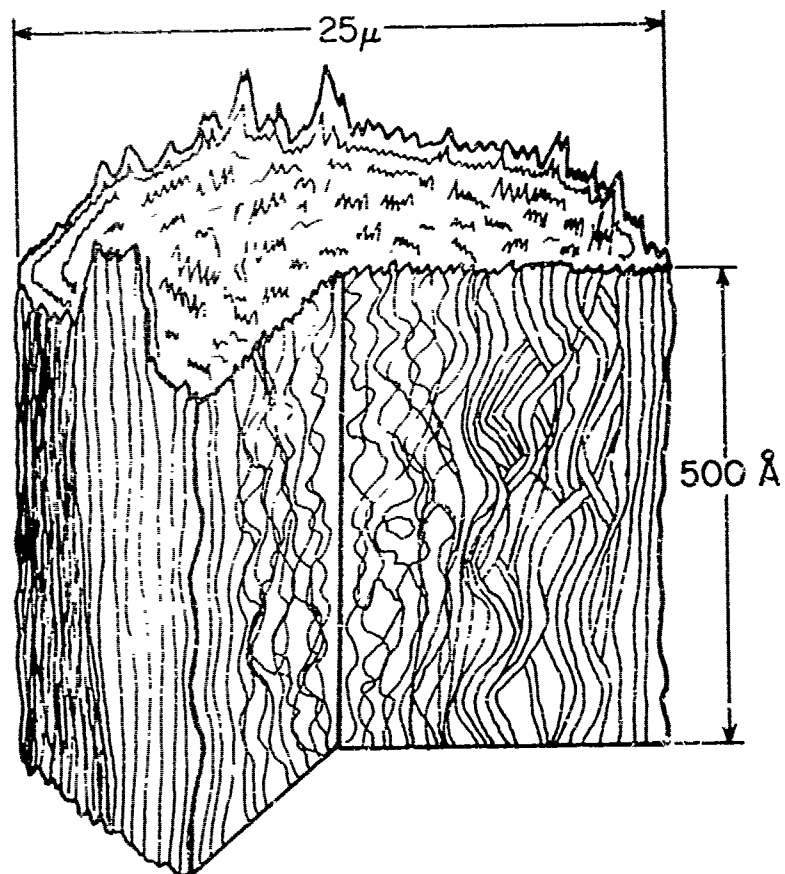
#### C. G. E. Monofilament Characterization

This  $\approx 25\mu$  diameter monofilament is produced from a polyacetylene precursor having a char yield of about 90% and has high performance properties<sup>4</sup>; its structural model is given in Fig. 17. From corrected x-ray results the  $d_{0002}$  was determined as  $3.395\text{\AA}$  while  $l_c$  was  $104\text{\AA}$ . Quantitative determinations of basal axial preferred orientation indicate that the elastic tensile modulus should be in the 60-90 Msi range based on similar measurements of rayon and PAN precursor materials. While the axial preferred orientation and  $l_c$  are reasonably high, no three dimensional lines were observed. Dark field (0002) electron microscopy revealed the basic structural unit has the rippled ribbon morphology, and that  $l_c$  is about  $100\text{\AA}$ , in agreement with x-ray results. As with other carbon fibers, the ribbon length appears to extend at least into the micron range. Optical characterization shows the radial preferred orientation is onion skin, with the axial preferred orientation being greatest at the outside of the fiber.

### PART 2. General Studies of Carbon Fibers

#### A. Density Results

Fig. 18 is a plot of uncorrected fiber elastic modulus versus density. When the curves are drawn connecting fibers of the same precursor as shown, several unusual features are observed.



G.E. Monofilament

Fig. 17 Three-Dimensional Structural Model



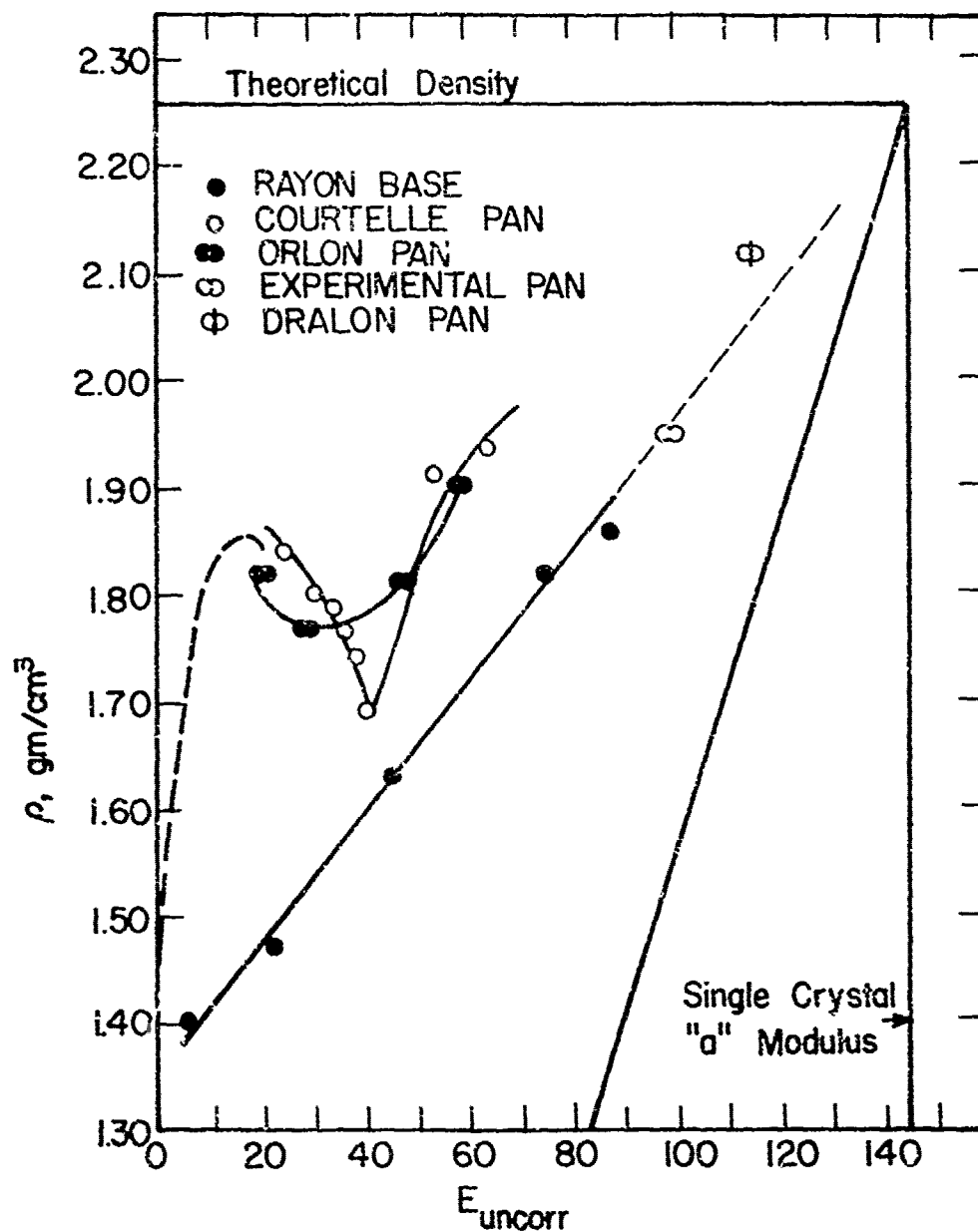


Fig. 18 Modulus vs. Density of a Wide Range of Carbon Fiber

A pronounced minimum occurs for the Courtelle and Orlon type fibers at about 40-45 Msi. A drop also occurs for the rayon fibers as well but in a much higher modulus region.

An upper bound for fiber elastic modulus as a function of density has been calculated by assuming perfect orientation of the basal planes parallel to the fiber axis with any porosity also considered as being in parallel. While a fiber with this microstructure may be undesirable for other reasons, the limit does provide an estimate of the highest modulus obtainable for a given density. Hence, a measure of elastic modulus efficiency may be obtained by dividing the modulus of a given fiber by the upper bound limit for the given fiber density. A lower bound for the elastic modulus, corresponding to any porosity being distributed in series, cannot be made without postulating a fiber model. This development will be described in the future reports.

Fig. 19 shows the variation in basal spacing,  $d_{0002}$  as a function of modulus; again, points for a common precursor were connected. As modulus increases the interplanar spacing drops smoothly for the rayon fibers, with the exception of the catalytic-

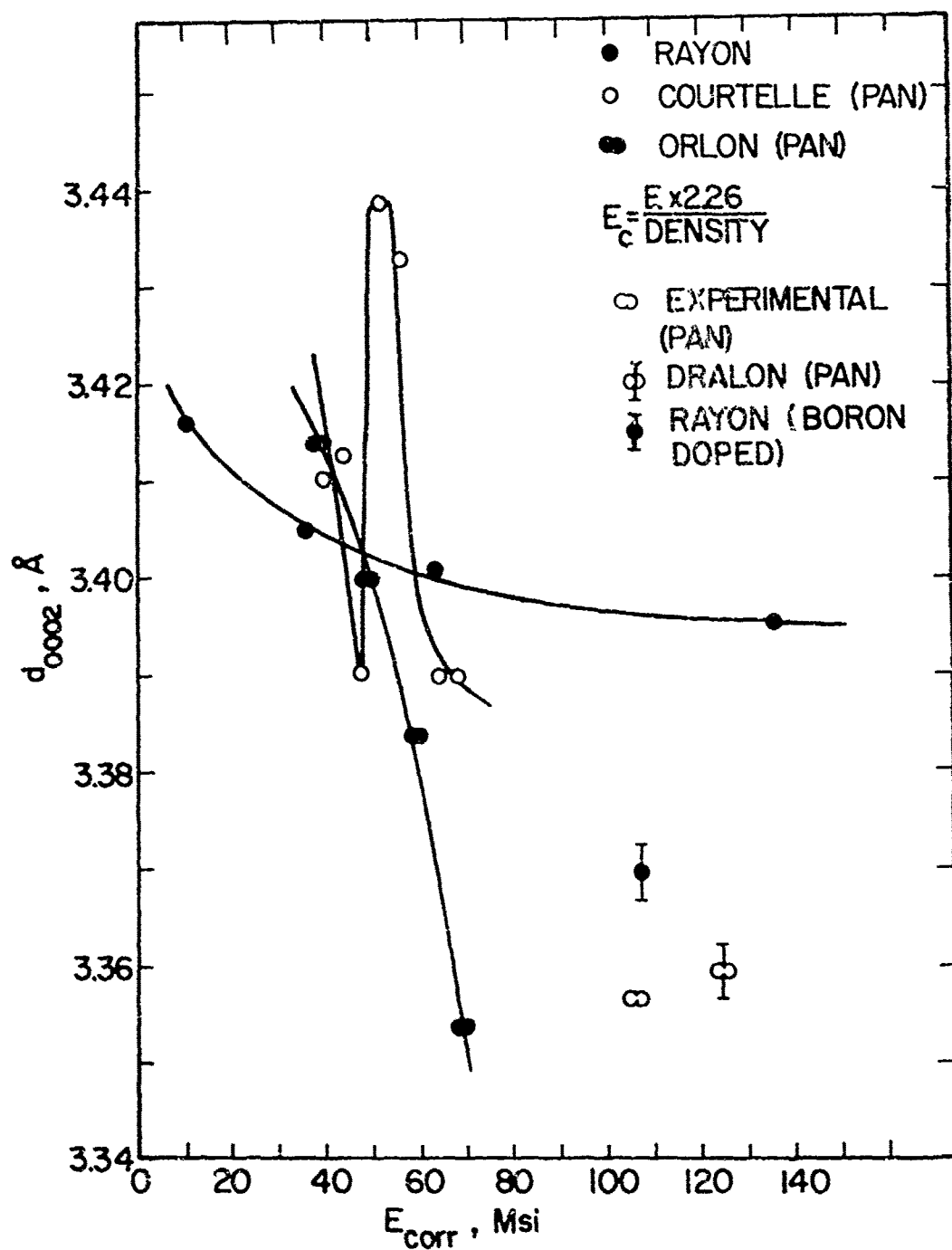


Fig. 19 Basal Spacing,  $d_{0002}$ , vs. Modulus of Fibers

cally graphitized CS-4 which is much more graphitic than the others. The orlon fibers from 3T through 6T also become progressively graphitic at a faster rate than rayon. The situation for the Courttelle fibers is erratic. The  $d_{0002}$  drops from about  $3.41\text{\AA}$  as E rises from 40 to 47 Msi; then it increases rapidly to  $3.44\text{\AA}$  as E reaches 51 Msi. Subsequently, it drops rapidly in a uniform fashion.

The stack height,  $l_c$ , as a function of modulus for each precursor type is given in Fig. 20. Again, with the exception of the catalytically treated CS-4, the crystallite size increases uniformly for the rayon base fibers. The same appears to be true, though to a somewhat lesser extent, for the dogbone fibers. The behavior for the Courttelle fibers again is anomalous in the same region where the density and interplanar spacing deviate.

Viewed in a different way, Fig. 21, is atomic basal spacing  $d_{0002}$ , as a function of crystallite stack height,  $l_c$ . For the rayon fibers  $l_c$  increases uniformly as  $d_{0002}$  decreases with the exception of the boron catalysed sample CS-4. As  $d_{0002}$  drops for the orlon fibers,  $l_c$ , increases in an almost linear fashion till the material becomes almost totally graphitic.

If the curve for the Courttelle fibers is drawn connecting points in order of increasing tensile modulus, the relationship is seen to be very complex. As the modulus rises from AS and Morganite II to CS-7,  $d_{0002}$  drops and the crystallite size increases;

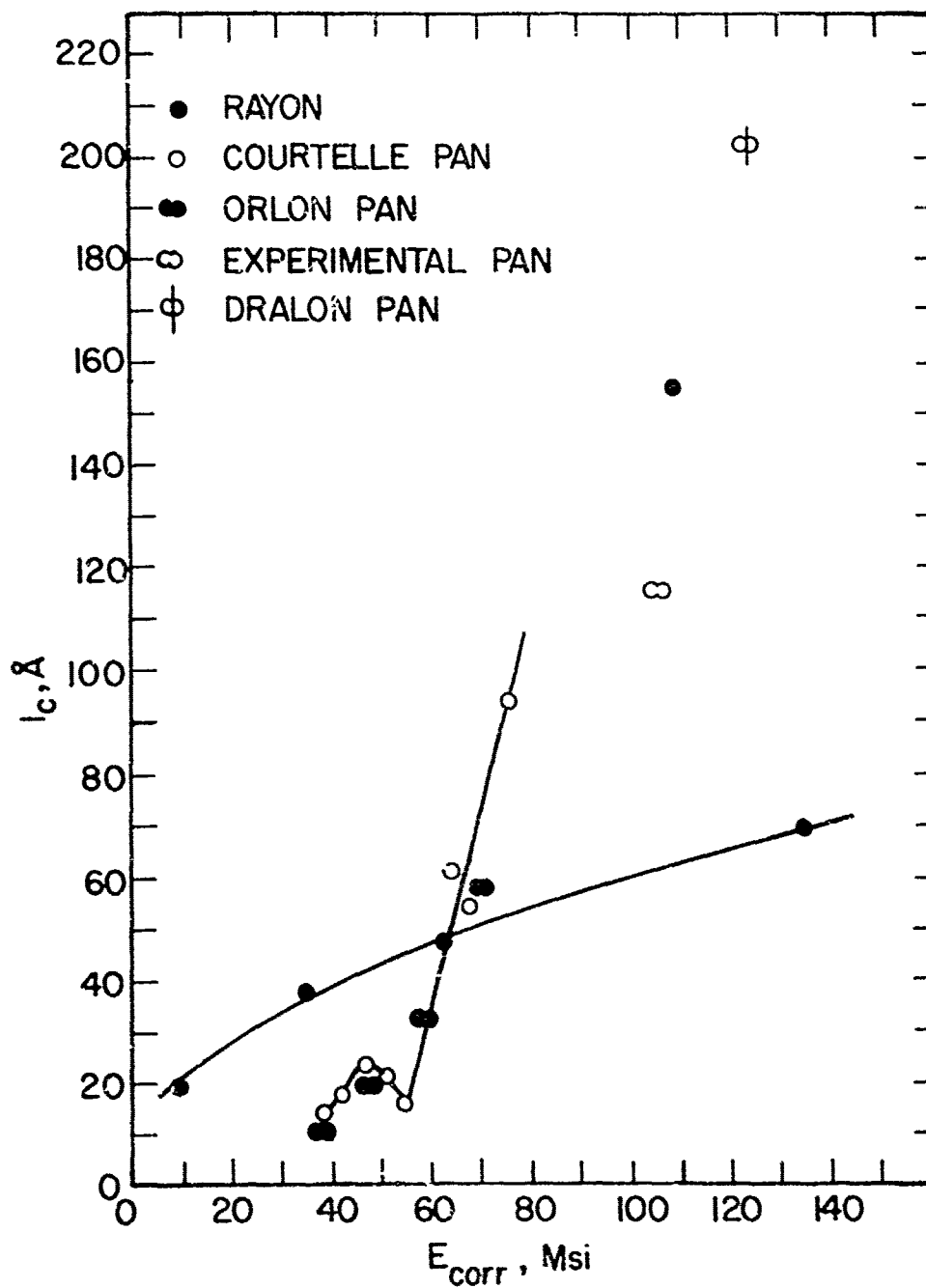


Fig. 20 Basal Stack Height,  $l_c$ , vs. Fiber Modulus

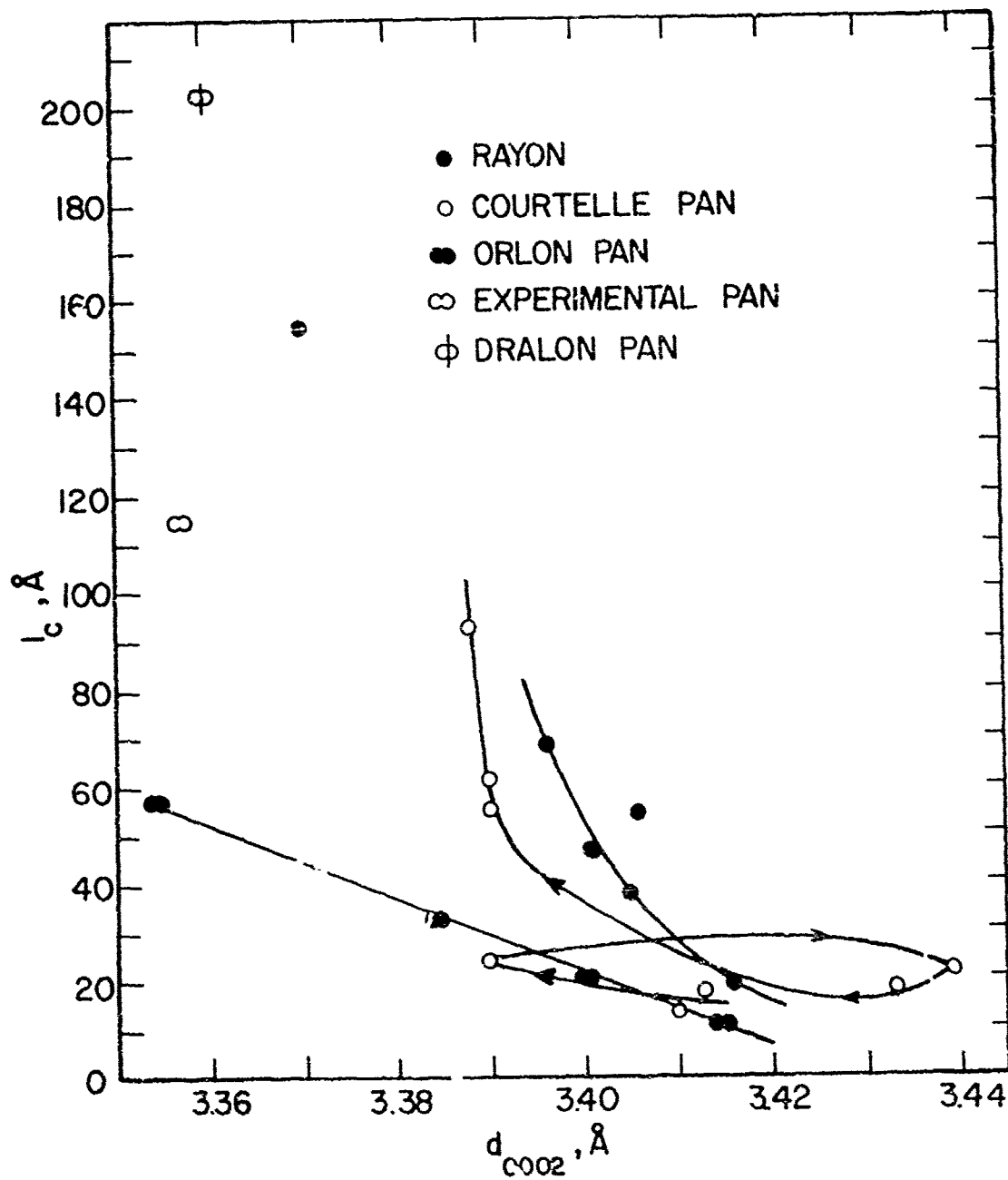


Fig. 21 Basal Stack Height,  $l_c$ , vs. Basal Spacing,  $d_{0002}$

further relatively small increases in modulus are not followed by decreasing interplanar spacings, but by the opposite. After the modulus rises above 40 Msi as in HTS and CS-2 the interplanar spacing drops rapidly followed by a stalling at about  $3.39\text{\AA}$  as the stack height rises.

Given in Fig. 22 is a plot of elastic modulus, corrected for density, as a function of the index of preferred orientation,  $W_{1/2}$ . As modulus increases in the rayon series,  $W_{1/2}$  drops in a uniform fashion; the same is true for the orlon fibers. However, for those Courtelle base fibers which are in the vicinity of the density,  $l_c$ , and  $d_{0002}$  anomalies, there is a much higher degree of scatter of the points. Another general feature is that the rayon base fibers have higher average axial preferred orientations for a given modulus (below  $E \approx 80$  Msi) than do the PAN fibers.

The bulk parameters, such as density and x-ray indices for the rayon and orlon samples having corrected moduli up to about 100 Msi, behave in a more-or-less uniform fashion. As modulus increases, density increases, basal spacing drops, and  $l_c$  size increases. For the Courtelle fibers, anomalies exist; of most significance is the fact that the erratic behavior corresponds to the region marking the onset of the drop in strength with increasing elastic modulus.

As a minimum in the bulk density occurs, the basal plane spacing fluctuates as does the size of the basal stack; furthermore,

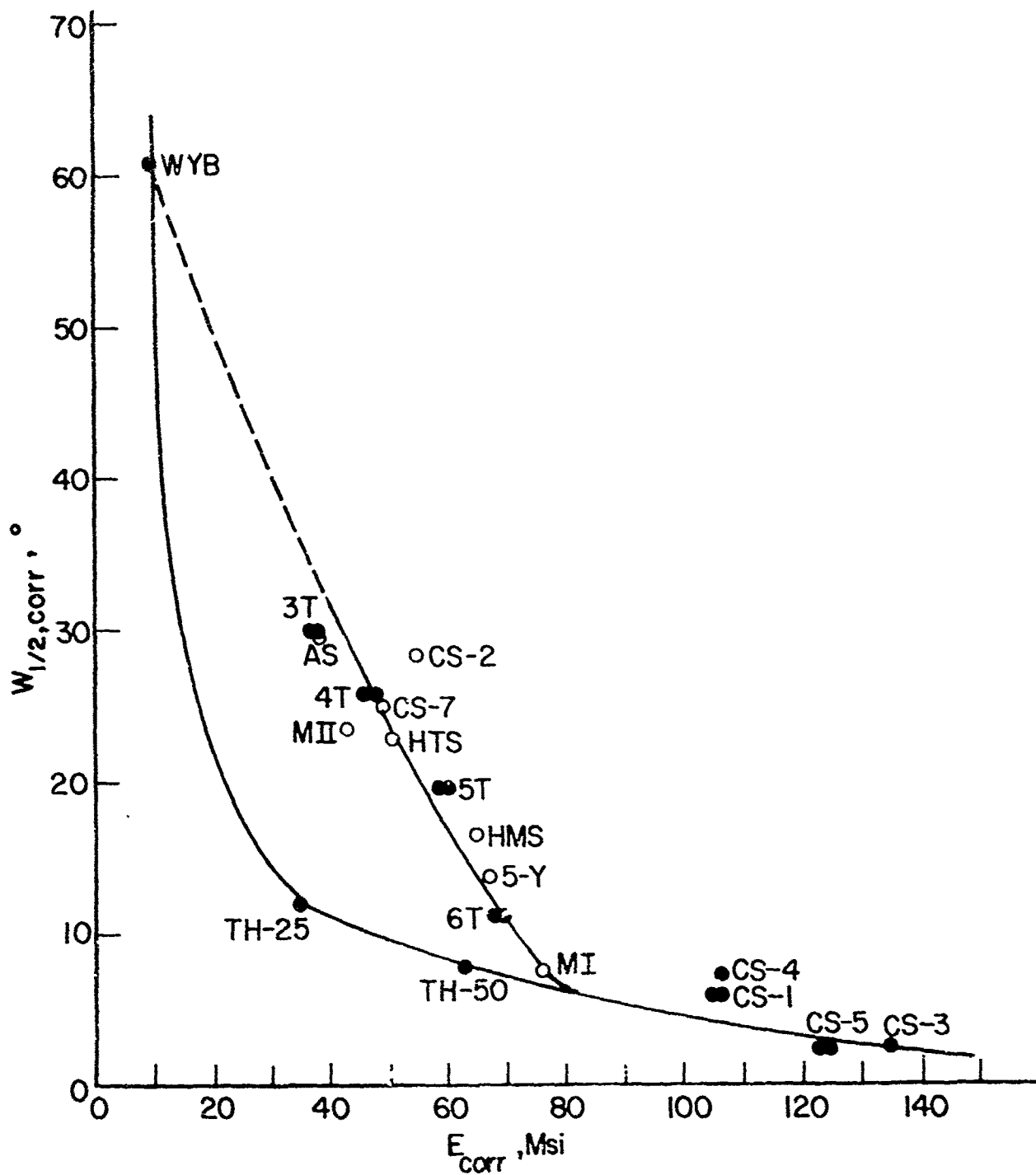


Fig. 22 Index of Preferred Orientation,  $W_{1/2}$  vs. Fiber Modulus



an instability in the index of axial preferred orientation,  $W_{\frac{1}{2}}$ , occurs. In fact, in the modulus progression from Morganite II ( $E_{\text{corr}} = 43 \text{ Msi}$ ) to CS-2 ( $E_{\text{corr}} = 55 \text{ Msi}$ ), there is a drop in axial preferred orientation.

In any case however, it is apparent that for the same corrected elastic modulus, the hot stretched fibers have higher axial preferred orientations than do the PAN base materials. The implication is that the state of stress within the PAN fibers has a significant component resulting from constant strain conditions. From a structural standpoint this would imply that, for a given preferred orientation, more tangling of the micro-ribbons occur such that adjacent ribbons restrain each other under fiber tensile load. Whether the structural source of the restraint is due to a purely geometrical effect, or inter-ribbon bonding is not clear at this point. However, the anomalies in basal spacing, stack thickness, and density are thought to be related, but the relationship is observed by residual stresses generated on cool-down from final heat treatment temperatures. It has been calculated by <sup>6</sup> LeMaistre that the magnitude of such stresses is of the order of the strength of graphite in the "c" direction. Additional preliminary calculations of the magnitude of circumferential compressive stresses generated on cool-down in the interior of circular cross-section fibers however lend support to the generation of internal flaws via shear; i.e. compressive buckling in the fiber interior. In any case however, both models imply a processing

region of structural instability. Furthermore, such models also lend support to optical results, which suggest that the rippled ribbons may more properly be described as rippled sheets. It is interesting to note that HTS and CS-7 (early HTS) have radically different values of  $d_{0002}$ . Assuming that production procedures have changed only a little, the structures present in such fibers may be very highly strained, and relatively small changes in final heat treatment temperature or rates of heating, may make a difference.

Additions of boron in the catalytically graphitized fibers promotes graphitization; for the same modulus, the basal spacing is lower and the stack thickness greater.

### PART 3. Organic Fibers

The organic fibers which were studied include:

1. PRD-49-I
2. PRD-49-III
3. PRD-49-IV
4. Old Fiber B
5. New Fiber B

Property information which was supplied by the Air Force is based on duPont and AFML generated data.

TABLE II  
DU PONT AROMATIC POLYAMID YARN PROPERTIES \*

	Fiber			
	PRD-49-I	III	IV	B
Tensile Strength x $10^3$ psi	350	400	430	205
Modulus x $10^6$ psi	19-21	19	12	8.2
$E_{corr}$	20	19	12	8
Elongation, %	1.5-2.0	2.0	3.3	6.5
Density, g/cc	1.48	1.45	1.45	1.44
Moisture Regain, %	0.72	1.5	4.0	5.0
Denier	400-650	195-380	200-400	740

\* Based on duPont and AFML generated data.  
Courtesy J. Ray, AFML.

A PRD-49-I/epoxy composite, which had been tested to failure in compression in the direction of the fiber axes was also examined. An optical micrograph of a polished cross-section of the main faulted zone within this sample is shown in Fig. 23. The plane of this zone is at about  $45^\circ$  to the principle compressive stress axis. If the fibers away from this faulted zone are viewed at higher magnification and in reflected polarized light, with the fiber axes parallel to the analyzer, more detail emerges as shown

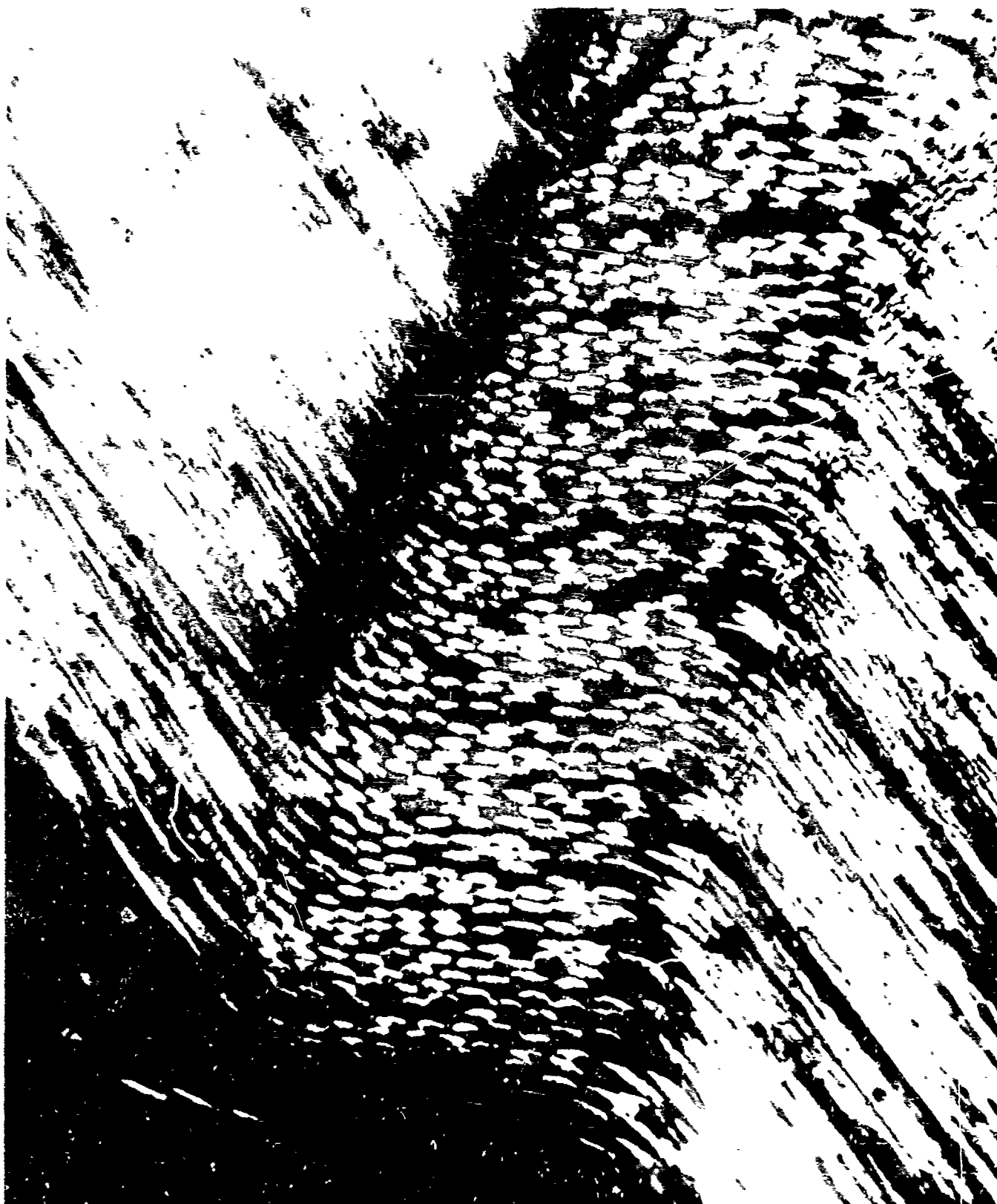


Fig. 23 Optical Micrograph Failure Zone in Compression  
Tested PRD-49-I - Epoxy Composite, 1 cm  $\approx$  100 $\mu$

in Fig. 24. Lines of high optical activity at  $45^\circ$  to the fiber axes arise. The density of these lines increases as the distance from the faulted zone decreases. Finally, shown in Fig. 25 is a bright field profile of a fractured end of a single PRD-49-I fiber taken with a Hitachi model HS-7 electron microscope. The very jagged profile is indicative of a very highly aligned, anisotropic structure. X-ray pinhole photograph of bundles of the aligned fibers were taken; given in Fig. 26 is the diffraction pattern of PRD-49-I, and in Fig. 27 that of Fiber B. Only these two are presented, since they are representative of the extremes in elastic modulus. The PRD-49-I pattern indicates that this fiber is paracrystalline, while Fiber B is much less developed, but does definitely have a marked axial preferred orientation.

Differences in radial textures are also present in the organic fibers. Fig. 28 is a montage of micrographs of polished cross sections of the fibers mounted in epoxy. The fibers are arranged in order of increasing elastic modulus with the exception of the newer Fiber B sample which has been placed at the end, since no tensile data was available at the time of this writing; it is apparent that this newer sample belongs between PRD-49-I and the older Fiber B however.

One of the differences apparent is that III, IV and new Fiber B have what appear to be cracks present. In an effort to determine whether these cracks were present in the samples or



1. The first step in the process is to identify the problem or issue that needs to be addressed. This involves gathering information and understanding the context of the problem.



Fig. 25 Electron Bright Field, PRD-49-I  
Fracture Profile, 1 cm  $\approx$  0.6 $\mu$

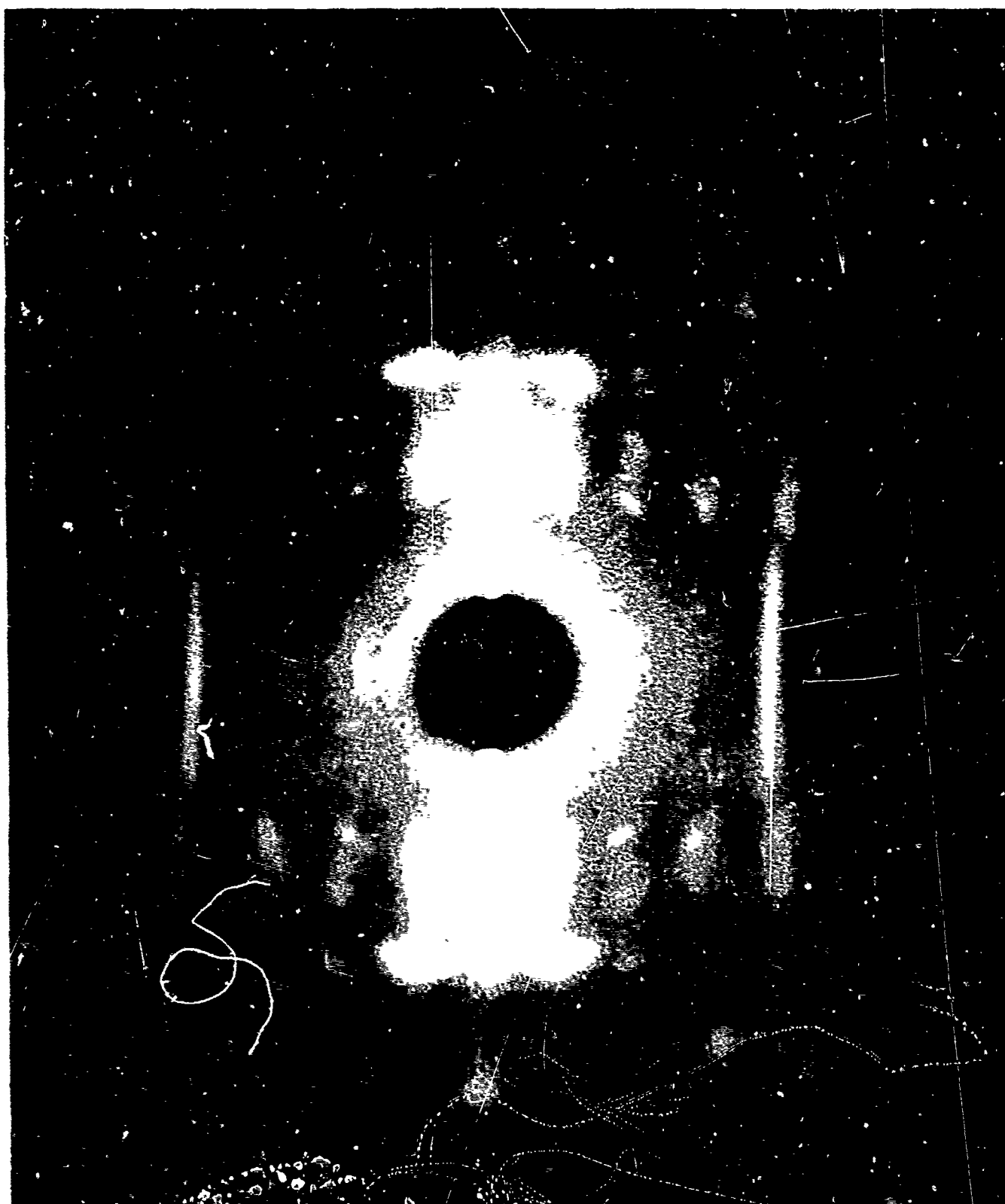


Fig. 2 X-ray Pinhole Photograph of a  
Collimated Bundle of FRD-40-T Filaments



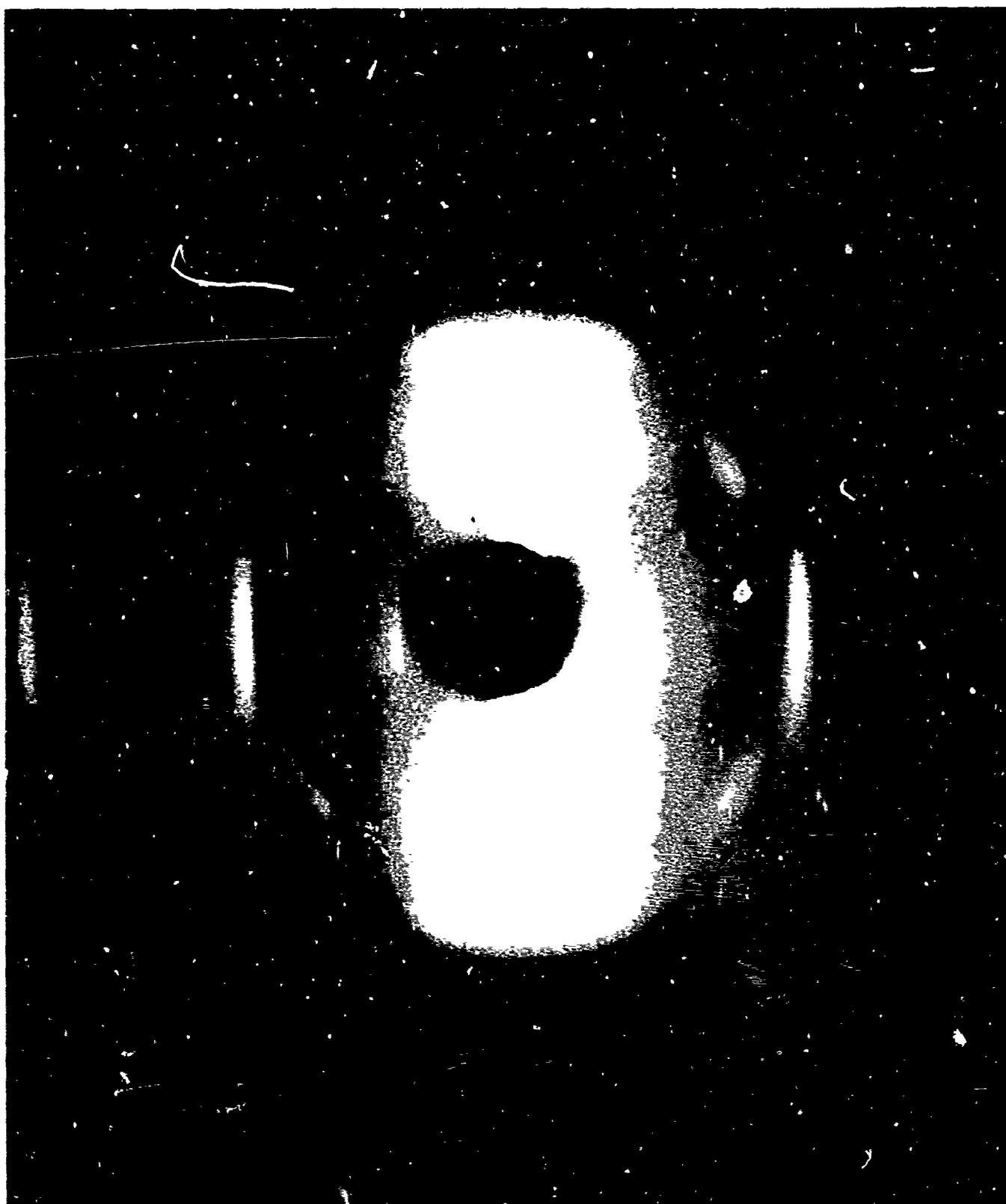
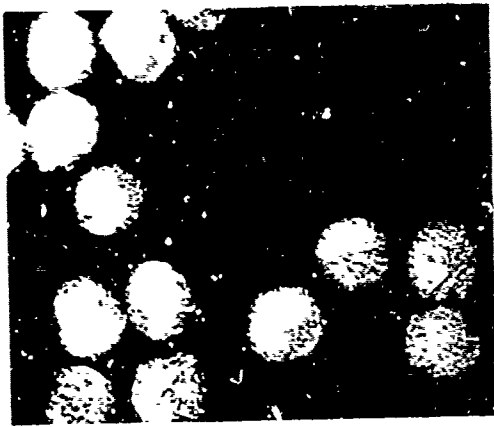
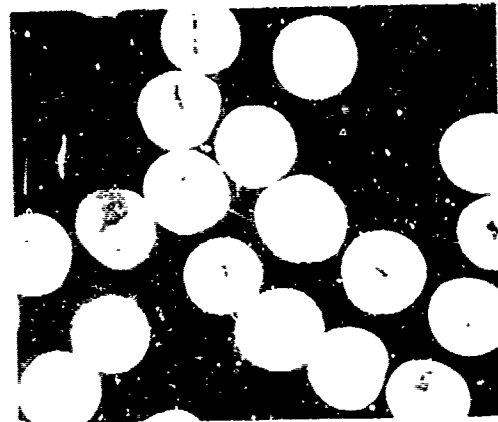


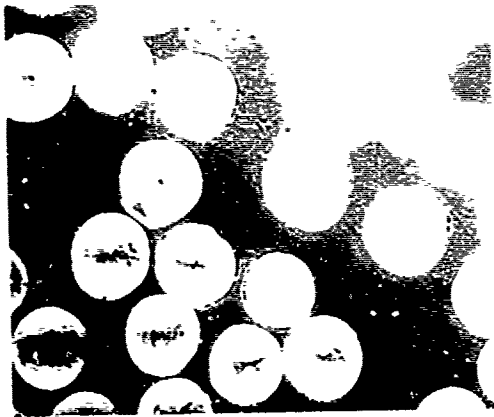
Fig. 27 X-Ray Pinhole Photograph of a  
Collimated Bundle of Filter Filters



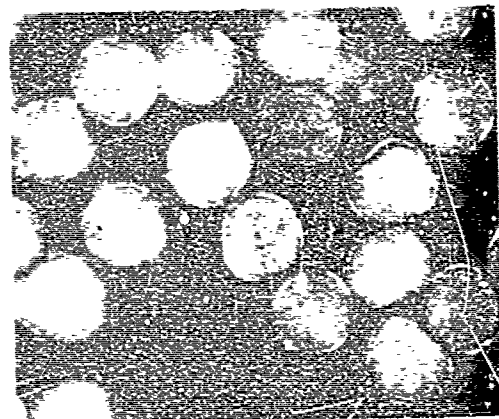
Early Fiber B  
E = 8 Msi



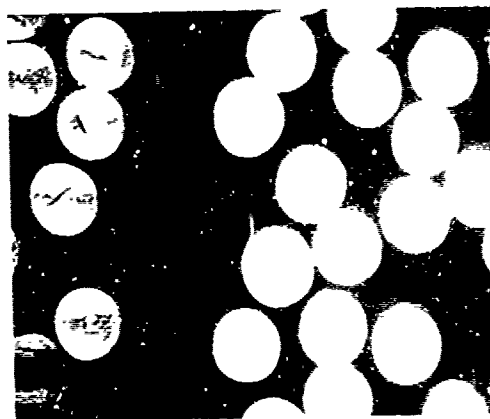
PRD-49-IV  
E = 12 Msi



PRD-49-III  
E = 19 Msi



PRD-49-I  
E = 20 Msi



New Fiber B

Fig. 28 Montage of Optical Micrographs of Polished Cross Sections of Organic Fibers in Reflected Polarized Light, 1 cm  $\approx$  10 $\mu$

were induced by specimen preparation, each of the samples was polished in one direction in the final stages of mechanical polishing. Observations indicated that the cracks then were parallel to the polishing direction for samples III, IV, and the newer Fiber B. In the case of the old Fiber B and PRD-49-I, there was optical anisotropy of the whole bundle of fibers. The fiber bundle anisotropy was characterized by an optical extinction angle similarly to single fibers. The results are:

<u>Fiber</u>	<u>Induced Bundle <math>A_R</math></u>	<u>Cracks Present</u>
Fiber B	$16^\circ \pm 1$	None
PRD-4 -IV	$\approx 0^\circ$	Many
PRD-49-III	$\approx 0^\circ$	Many
PRD-49-I	$20^\circ \pm 2^\circ$	None
New Fiber B	$< 5^\circ$	Some

Thus, two deformation modes are present. For Fiber B and PRD-49-I, deformation appears to be plastic, while III, IV, and the newer Fiber B behave more like brittle materials.

Such behavior suggests that while tensile behavior of PRD-49-I may be spectacular, compressive strength of composites will be very low; machinability and toughness will be anisotropic. The same comments are true for older Fiber B with the differences of lower modulus and strength. The increased radial brittleness of PRD-49-IV, III, and the newer Fiber B, will impart a higher fiber compressive strength, thus improving overall composite performance.

#### Summary of Organic Fibers

Of the organic fibers studied, PRD-49-I has the highest elastic

modulus, and Fiber B the lowest. In fact, the pinhole diffraction indicates that PRD-49-I is paracrystalline. Failure in compression is via shear at  $45^\circ$  to the principle compression axis; i.e., along the maximum shear stress plane, and is observable as oblique strain markings in reflected polarized light. This implies that the molecular chains are very highly aligned and have little bonding between adjacent linear elements. This poor coupling between chains is also responsible for the ease with which optical anisotropy may be introduced into a bundle - the same is true for Fiber B. In comparison, PRD samples III and IV, and the newer Fiber B are more brittle in a radial direction - polishing produces internal cracks. The shear strength in compression is probably higher, and thus also the composite compressive strength; however the tensile moduli of these fibers is lower.

## REFERENCES

1. Brydges, W. T., Badami, D. V., Joinier, J. C., and Jones, G. A., "On the Structure and Elastic Properties of Carbon Fibers", Am. Chem. Soc., Div. Poly. Chem., Atlantic City Meeting, Sept. 1968.
2. Heckman, F. A., "Microstructure of Carbon Black", Rubber Chem. and Tech. 37, 1245 (1964).
3. Diefendorf, R. J. and Tokarsky, E. W., "The Relationships of Structure to Properties in Graphite Fibers", Part I, AFML-TR-72-133, October, 1971.
4. Flom, D. G., Garowitz, B., Krutchen, C. M., Roberts, B. W., and Sliva, D. E., "Exploratory Development of High Strength, High Modulus Graphite Filaments", AFML-TR-72-24, Jan., 1972.
5. Reynolds, W. N., Physical Properties of Graphite, Elsevier Publishing Co. Ltd. (1968).
6. LeMaistre, C. W., "The Origin of Structure in Carbon Fibers", Ph.D. Thesis, Rensselaer Polytechnic Institute, Sept. 1971